Journal of Computational Neuroscience 19, 263–289, 2005

DOI: 10.1007/s10827-005-2288-5

Two Cortical Circuits Control Propagating Waves in Visual Cortex

WENXUE WANG
Department of Electrical and Systems Engineering, Washington University, St. Louis, MO 63130, USA
ww1@zach.wustl.edu

CLAY CAMPAIGNE
Committee on Computational Neuroscience, The University of Chicago, 1025 E. 57th Street, Chicago, IL 60637, USA

BIJOY K. GHOSH
Department of Electrical and Systems Engineering, Washington University, St. Louis, MO 63130, USA
ghosh@netra.wustl.edu

PHILIP S. ULINSKI
Committee on Computational Neuroscience, The University of Chicago, 1025 E. 57th Street, Chicago, IL 60637, USA
pulinski@uchicago.edu

Received December 20, 2004; Revised May 10, 2005; Accepted May 16, 2005

Action Editor: Jonathan D. Victor

Published online: 28 October 2005

Abstract. Visual stimuli produce waves of activity that propagate across the visual cortex of fresh water turtles. This study used a large-scale model of the cortex to examine the roles of specific types of cortical neurons in controlling the formation, speed and duration of these waves. The waves were divided into three components: initial depolarizations, primary propagating waves and secondary waves. The maximal conductances of each receptor type postsynaptic to each population of neurons in the model was systematically varied and the speed of primary waves, durations of primary waves and total wave durations were measured. The analyses indicate that wave formation and speed are controlled principally by feedforward excitation and inhibition, while wave duration is controlled principally by recurrent excitation and feedback inhibition.

Keywords: inhibitory interneurons, recurrent excitation, feedback, inhibition

Introduction

An interesting feature of turtle visual cortex is that visual stimuli produce waves of activity that originate near the rostral pole of the cortex and then propagate across the cortex to its caudal pole. These waves have been demonstrated using both multielectrode arrays and voltage sensitive dyes (Prechtl et al., 1997, 2000; Senseman, 1999). Both methods detect the activity of populations of pyramidal cells (Senseman, 1999). Propagating waves with comparable properties can be produced in a large-scale model of turtle visual cortex

that contains geniculate and cortical neurons (Nenadic et al., 2003). Analysis of waves in both real and model cortices using a variant of principal component analysis shows that information about the position of visual stimuli along the horizontal meridian of visual space is encoded in the spatiotemporal dynamics of the waves (Nenadic et al., 2002; Du et al., 2005). Understanding how cortical waves are generated and controlled by circuits of neurons in the visual cortex is, consequently, an important step in understanding how turtle visual cortex processes information.

This paper uses a large-scale model of turtle visual cortex to investigate the cellular mechanisms that control the formation and propagation of the waves. The model (Nenadic et al., 2003; Wang, 2006) contains neurons in the dorsal lateral geniculate complex of the thalamus and the five major populations of neurons in the visual cortex. Turtle visual cortex has three layers: an outer layer 1, an intermediate layer 2 and an inner layer 3 (Ulinski, 1999). It corresponds to the cytoarchitectonic area designated dorsal cortex, D, and is divided into lateral and medial parts, D_{L} and D_{M}, respectively. Pyramidal cells have somata situated in layer 2 and are the source of efferent projections from the cortex. The pyramidal cells in D_{L} and D_{M} differ morphologically and in their relationships to geniculate afferents. The cortex also contains at least three populations of inhibitory interneurons. Subpial cells have their somata and dendrites situated in the outer half of layer 1, embedded in afferents from the lateral geniculate complex. Stellate cells have somata situated in the inner half layer of 1. Horizontal cells have somata situated in layer 3. Interactions between these five types of cells involve four types of neurotransmitter receptors. Geniculate afferents are glutaminergic (Larson-Prior et al., 1991; Blanton and Kriegstein, 1992) and access the α-amino-3-hydrozy-5-methyl-4-isoxazole proprionic acid (AMPA) subtype of glutamate receptor. Pyramidal cell afferents are also glutaminergic (Larson-Prior et al., 1991; Blanton and Kriegstein, 1992) and access both the AMPA and N-methyl-D-aspartate (NMDA) receptor subtypes of glutamate receptors. Subpial, stellate and horizontal cells are $\mathrm{GAB_A}$ergic and apparently access both the $\mathrm{GABA_A}$ and $\mathrm{GABA_B}$ subtypes of GABA receptors (Blanton et al., 1987; Blanton and Kriegstein, 1992).

The five types of cells can be thought of as forming two anatomically defined pathways within the cortex (Fig. 1). A *feedforward pathway* (Fig. 1A) involves the geniculate inputs that make excitatory, AMPAergic contacts on subpial, stellate and lateral pyramidal cells. The subpial and stellate cells make $\mathrm{GABA_A}$ergic and $\mathrm{GABA_B}$ergic contacts on the lateral pyramidal cells. Lateral pyramidal cells give rise to corticofugal efferents (Ulinski, 1986), but also bear recurrent collaterals that contact other lateral and medial pyramidal cells. These collaterals are glutaminergic and access both AMPA and NMDA receptors. A *feedback pathway* (Fig. 1B) involves the recurrent collaterals of both lateral and medial pyramidal cells, which make glutaminergic contacts on subpial, stellate and horizontal cells. Each of these populations of inhibitory interneurons make GABAergic contacts on pyramidal cells. In addition, there are inhibitory contacts between individual

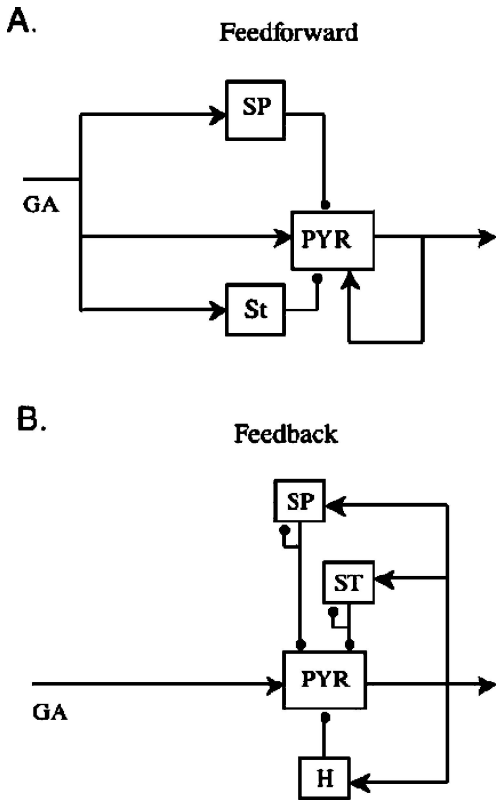

Figure 1. This figure shows the structure of anatomically defined feedforward (A) and feedback (B) pathways. Each box symbolizes a population of cells. The geniculate afferents (GA) provide excitatory input to cells in both pathways. The pyramidal cells (PYR) are excitatory. The distinction between medial and lateral pyramidal cells is not made in this diagram. The subpial (SP), stellate (ST) and horizontal (H) cells are inhibitory. The axons of pyramidal cells leave the visual cortex to other cortical areas and to the brainstem in both pathways.

subpial cells as well as between individual stellate cells. Both the lateral and medial pyramidal cells give rise to efferents to the thalamus, striatum and brainstem.

The functional roles of the feedforward and feedback pathways in controlling the formation and propagation of cortical waves were examined in this study. The maximal conductances of the glutaminergic and GABAergic synapses formed by each type of cell in our large-scale model were varied systematically and the speed and duration of cortical waves produced by simulating the responses of the cortex to 150 ms whole retinal flashes were measured. The detailed interactions between neurons in each pathway were then characterized by plotting the activity patterns for cells following manipulations of synaptic strengths in the two pathways. The simulations indicate that the two pathways control different aspects of wave formation and propagation. The formation and speed of propagating waves are controlled by feedforward excitation mediated by geniculate afferents and lateral pyramidal cells and inhibition mediated by subpial cells. The duration of waves is controlled by recurrent excitation mediated by the collaterals of both lateral and medial pyramidal cells and by feedback inhibition to both lateral and medial pyramidal cells. These effects are mediated principally by stellate and horizontal cells. Analysis of the information encoding properties of the waves indicates that the information content of waves is relatively independent of the strengths of individual categories of synapses and the speeds and durations of the waves.

Materials and Methods

Large Scale Model

The structure of our large-scale model is described in detail by Nenadic et al. (2003) and by Wang (2006). In brief, individual neurons were assigned spatial distributions corresponding to the anatomically determined distribution of neurons in turtle visual cortex. Neurons were distributed on a grid such that the relative densities of neurons in each of the three layers of the cortex were preserved (Fig. 2A). The model had 368 lateral pyramidal cells, 311 medial pyramidal cells, 44 subpial cells, 45 stellate cells, 20 horizontal cells and 201 geniculate neurons. Each neuron was represented by a compartmental model with 12–29 compartments based on its morphology as seen in Golgi preparations or neurons filled with Neurobiotin. Biophysical parameters were constrained using the responses of neurons following intracellular current injections. Each neuron had a spike generating mechanism implemented using Hodgkin-Huxley-like kinetic schemes. In addition, models of lateral and medial pyramidal cells and subpial cells had a high threshold calcium conductance and a calcium dependent potassium conductance that were responsible for spike rate adaptation in the pyramidal cells. Geniculate neurons were single compartments with a spike generating mechanism. Geniculate axons were implemented as delay lines with conduction velocities constrained by the experimentally measured conduction velocities of geniculate axons. Synapses were modeled as synaptic currents. Simulations were implemented in the neuronal simulation software package, *Genesis* (Bower and Beeman, 1998).

Simulations

Diffuse retinal flashes were simulated by simultaneously injecting square current pulses of 150 ms duration into all 201 geniculate neurons. Spots of light presented at positions at the left end, the center and the right end of the horizontal meridian of visual space were simulated by injecting square current pulses of 150 ms duration into geniculate neurons 1–20, 91–110 and 181–200, respectively. These latter simulations were carried out by injecting a Gaussian white noise with amplitudes ranging from -6 nA to $+6$ nA and a mean of 2 nA. Stimuli were repeated 100 times for each position and each synaptic strength. Responses of the visual cortex were simulated for 1,500 ms. The role of each type of cell and each receptor subtype in controlling cortical waves was investigated by systematically varying the maximal conductances of the glutaminergic and GABAergic conductances formed by each type of cell. Separate simulations were carried out in which synapses onto and from both lateral and medial pyramidal cells, only lateral pyramidal cells, and only medial pyramidal cells were varied. The maximal conductance of the glutaminergic and GABAergic synapses were varied from 0% through 150% in steps of 10%. The 100% values for the GABAergic synapses formed by subpial cells on pyramidal cells were 3.0 nS. The 100% values for all of the other types of synapse were 5.0 nS. A total of 4,393 simulations were carried out and analyzed. Each simulation required about 2 h on a Dell Precision Workstation with 1 Gbyte of RAM and a 1 GHz processor speed.

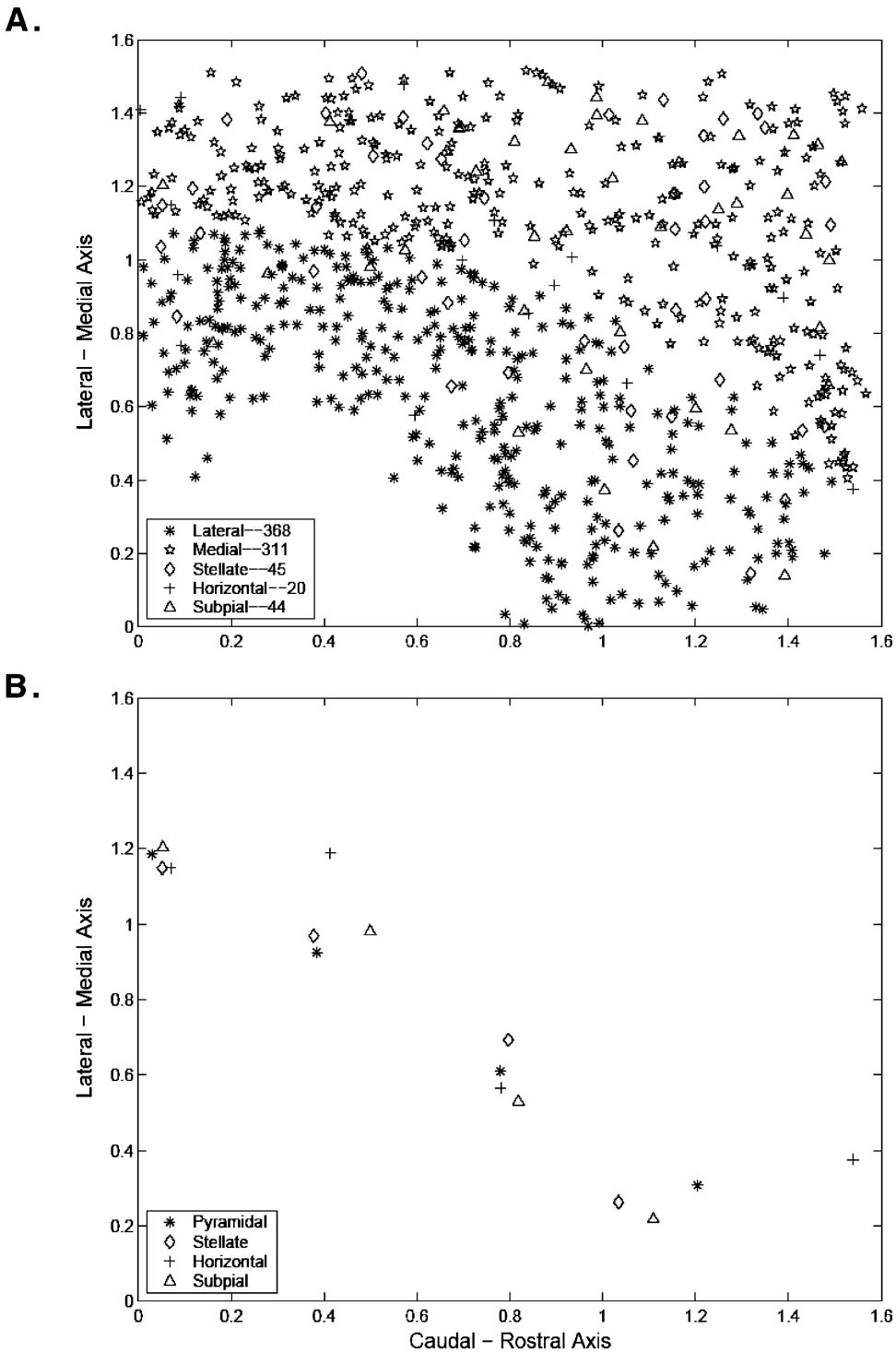

Figure 2. Spatial distribution of neurons in the large-scale model of visual cortex. (A) The positions of all of the cortical cells in the model. Different types of cells are indicated by different symbols. Cells are plotted on a 1.6 mm × 1.6 mm grid. (B) This plot is the same as A, except that it shows only the positions of cells along a diagonal that extends from the rostral-lateral corner of the cortex to its caudal-medial edge. The firing pattern of these cells are shown in Fig. 3.

Data Analysis

The voltage responses of the cortical neurons were represented as movies prepared using *Matlab*. Speed and duration were measured for each of 832 cortical waves. Senseman and Robbins (2002) report that the most accurate way to measure the speed of a propagating wave in the cortex is to plot the latency of the half-height of the wave front as a function of position along a transect across the cortex. These plots tend to be linear, so the propagation speed of waves was measured by dividing the length along a diagonal transect of the cortex by the half-height latency of the waves at the caudal-medial pole of the cortex. Two measures of wave duration were taken for most waves. Total duration is the time required for activity in the cortex to decline to its pre-stimulus level. An algorithm was devised to automatically measure the total durations of waves. This total response could typically be divided into a primary wave that propagated from the rostral pole of the cortex to its caudal pole, and a secondary wave that originated at the caudal pole (see below). It was not possible to devise an algorithm that would reliably measure the duration of the primary wave. Instead, it was necessary to visually inspect the movie resulting from each simulation and record the time at which the amplitude of the response at the caudal edge of the cortex reached a minimal value before generating a secondary wave. This time was the duration of the primary wave and is visible as a local minimum between two peaks in activity plots of pyramidal cells (e.g. Fig. 5A). The duration of the secondary wave was obtained by subtracting the duration of the primary wave from the total wave duration. In some cases, the cortical response consisted of an initial depolarization that did not propagate. These responses had a speed of 0 μm/ms.

In addition to characterizing the speed and duration of waves, the firing pattern for each individual neuron was obtained for different values of the maximal synaptic conductances. The output from each simulation is the membrane voltage of the soma compartment of each neuron as a function of time. These voltages were thresholded so that the response of each neuron was a vector of zeroes and ones. A value of 1 occurred if the soma voltage of the neuron was above the spike threshold during a 5 ms time bin; a value of 0 occurred whenever the soma voltage did not reach spike threshold in that time bin. The firing patterns for all of the neurons were displayed in space-time plots. Each space-time plot represents the firing pattern of individual neurons as a series of rows. The activity pattern for a given class of cortical neuron is a plot of the fraction of the total number of cells in the class that were active in each 5 ms time bin. The activity patterns of different classes of neurons can be directly compared because the activities are expressed as fractions, but it should be remembered that the total numbers of neurons in each class are quite different. Thus, 70% of the subpial cell population is a smaller number (31 cells) than 30% of the pyramidal cell population (204 cells).

A combination of Karhunen-Loeve and Bayesian estimation methods was used to characterize the coding properties of cortical waves using the simulations in which spots of light positioned at the left edge, center and right edge of the horizontal meridian of visual space were simulated. The procedure used follows that developed by Nenadic et al. (2002) and Du et al. (2005). These publications should be consulted for details. In brief, each wave was represented as a *Matlab* movie. The movie was decomposed into a series of space-dependent basis functions weighted by time dependent coefficients. The original movie could be faithfully represented using the first three basis functions, so that the time dependent behavior of the cortex could be represented in a three dimensional phase space (A-space) that was spanned by these coefficients. Each stimulus presentation resulted in a trajectory in A-space. Individual trajectories were then decomposed into a series of time-dependent basis functions weighted by space-dependent coefficients. A wave was, consequently, represented in a phase space (B-space) spanned by the second set of coefficients. Multiple presentations of a given stimulus produced a cluster of points on a plane in B-space. Bayesian estimation methods were then used to divide this plane into discrimination regions.

Results

Cortical Waves Have Three Components

A simulated light flash produces a wave of activity that begins at the rostral pole of the cortex and propagates towards the caudal pole. General features of the waves can be seen by examining the firing patterns of individual neurons at different points along a diagonal line that extends from the rostral-lateral edge of the cortex to its caudal-medial edge (Fig. 2B). Figure 3 shows the firing patterns of examples of subpial, pyramidal,

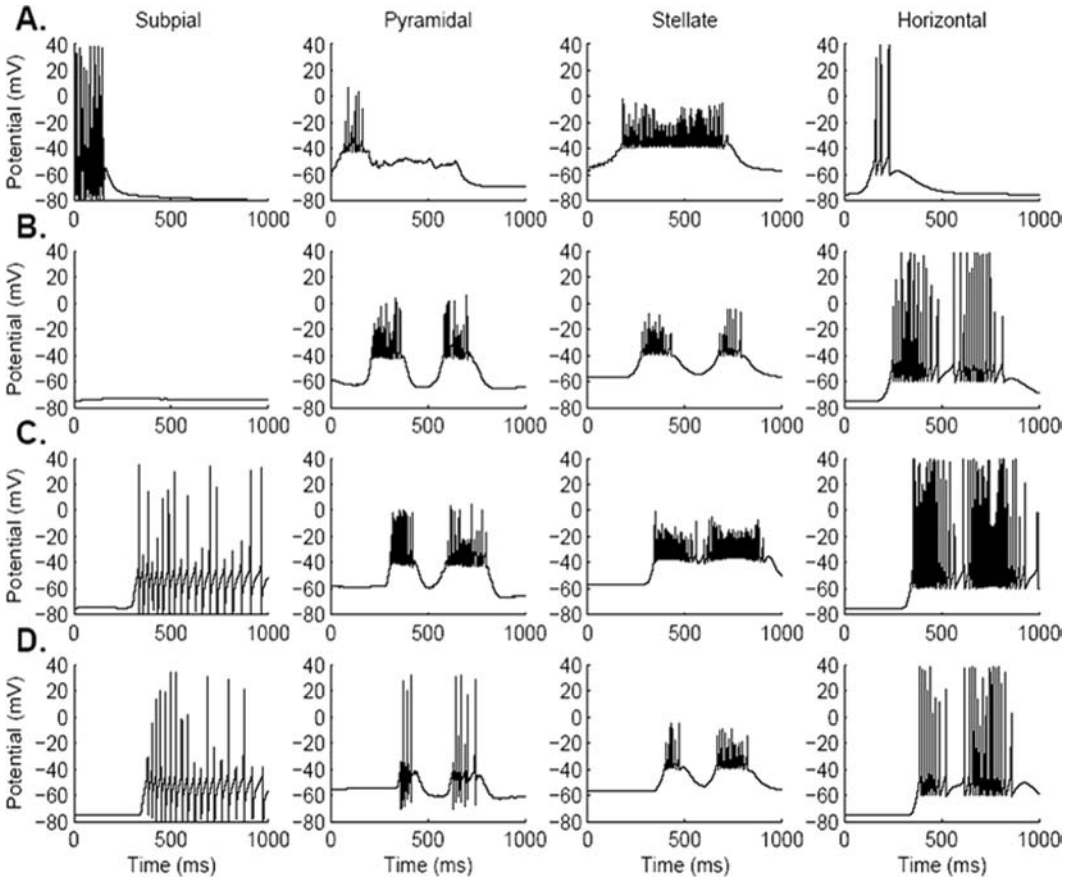

Figure 3. Firing patterns of cells along a diagonal transect across the model cortex. The firing patterns of the cells indicated in Fig. 2B are shown. Firing patterns of subpial, pyramidal, stellate and horizontal cells are shown in individual columns. Cells in rows (A) through (D) are positioned at different positions along the transect from the rostral-lateral corner of the cortex to its caudal-medial edge.

stellate and horizontal cells that lie along the transect shown in Fig. 2B. One major feature of the firing patterns is that there are distinct differences in the firing latencies of the four types of cells. Subpial cells fire earliest, followed by pyramidal cells, stellate cells and horizontal cells. Second, there is a systematic shift in latency for each type of cell along the transect. This reflects the propagation time required for the wave of activity to move across the cortex. Third, some cells do not generate action potentials. The majority of cells shown in Fig. 3 were selected to illustrate their firing patterns, but the subpial cell in row B is an example of a cell that does not generate action potentials in response to this particular stimulus. Fourth, the cells tend to fire in two bursts. This is most evident in the pyramidal, stellate and horizontal cells in rows B, C and D.

These examples of the firing patterns of individual cells can be compared to the behavior of each population of cells in a space-time plot (Fig. 4). The firing pattern of each individual cell is shown by a row of dots. Cells of each type are grouped together with subpial cells at the top of the plot and lateral pyramidal cells at the bottom of the plot. Cells within each population are ordered from the top of the plot to the bottom of the plot according to their positions along the transect. This plot shows the same four features that were noted in Fig. 3. Subpial cells, as a population, fire first, followed by lateral pyramidal cells, medial pyramidal cells, stellate cells and horizontal cells. Wave propagation is visible by the progressive shift in firing latencies for pyramidal, stellate and horizontal cells. The two bursts of firing are clear for each of the five populations of cells. The space-time plots also indicate that cortical waves can be divided into three components for the purpose of analysis. First, activation of geniculate afferents produces an initial depolarization in the rostral

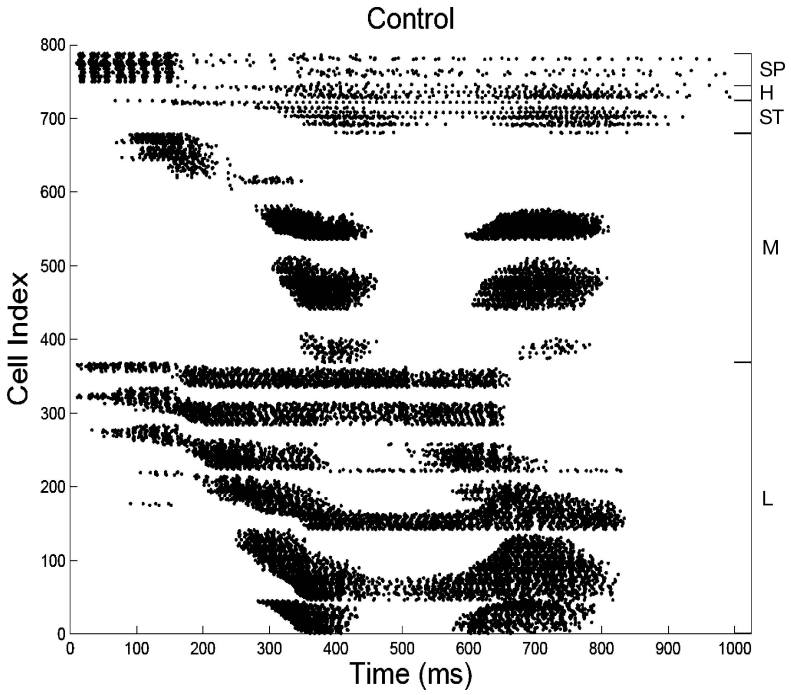

Figure 4. Space-time plot of the response of the model to a simulated 150 ms light flash. Each row of dots in this space-time plot indicates the occurrence time of a spike in an individual cell. Individual cells are numbered (Cell Index). Cells of the same type are grouped together in the plot, with subpial cells (SP) plotted at the top of the graph and followed by horizontal (H), stellate (ST), medial pyramidal cells (M) and lateral pyramidal cells (L). Cells of each type are ordered, approximately, according to their position along the transect. The slope of the leading edge of activity of the lateral pyramidal cells is an indication of the speed of the propagating wave.

pole of the visual cortex with a latency of about 20 ms after activation of geniculate neurons. If the strength of the activation is below threshold for initiation of a propagating wave, the depolarization will last for up to 200 ms. However, it remains localized within one region of the cortex and does not propagate across the cortex. Second, activation of geniculate afferents above the threshold for wave formation produces a primary wave that begins at the rostral pole around 200 ms after the stimulus. It then propagates across the cortex, reaching the caudal pole of the cortex at about 400 ms. In our model, the wave has a propagation speed between 3 μm/ms and 8 μm/ms, depending on the values of synaptic conductances used in a simulation. The wave begins to decline in amplitude after reaching the caudal pole of the cortex and dies out completely by about 600 ms after geniculate activation. Third, a secondary wave, or reflection, occurs in many, but not all, instances. The secondary wave appears as an increase in the amplitude of the wave after it has reached the caudal pole of the cortex. The secondary wave typically propagates back across the cortex towards the rostral pole and eventually subsides. The speed, trajectory and duration of the secondary waves are quite variable, but they usually die out between 800 and 1,500 ms after geniculate activation.

The same data can be represented in a different format by dividing the time axis into 5 ms bins and summing the total number of cells of each type active within a given time bin. The fraction of cells of each type that are active at a given time can then be plotted as a function of time (Fig. 5). A very small fraction of pyramidal cells becomes active about 20 ms after stimulus onset and gradually increases in size between 20 and about 200 ms as the initial depolarization forms (Fig. 5A). The primary propagating wave is then formed and is indicated by a linear increase in the fraction of active pyramidal cells, which reaches its maximum when the wave reaches the caudal pole of the cortex around 400 ms. The primary wave begins to decline in amplitude and reaches its minimum at about 600 ms, when the secondary wave begins to form. It reaches its peak around 750 ms and then declines to baseline by about 800 ms. A noteworthy feature of this

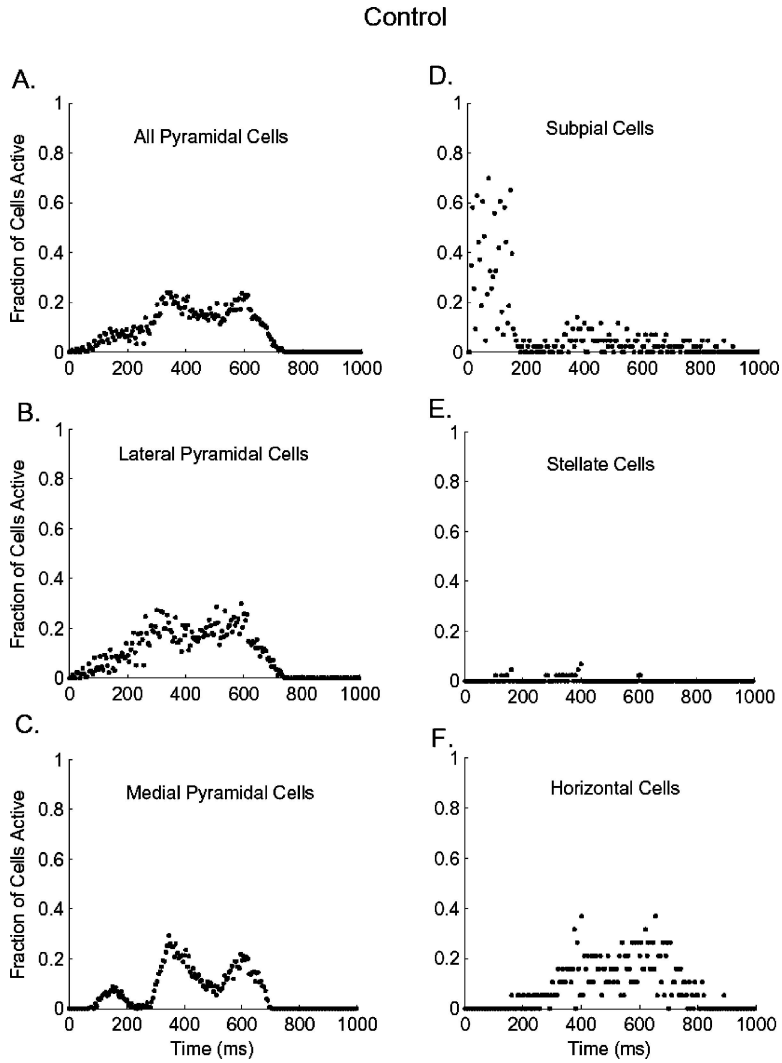

Figure 5. Activity patterns of populations of cortical neurons. These plots show the activity patterns of each of the five populations of cortical neurons in the model. Separate plots are shown for all pyramidal cells and for lateral and medial pyramidal cells. Each plot shows the fraction of the specified population of cells that are active in 5 ms time bins. The stimulus was simultaneous activation of all geniculate neurons for 150 ms.

activity pattern is that the majority of pyramidal cells are inactive at any given time during the response. The lateral (Fig. 5B) and medial (Fig. 5C) pyramidal cells have slightly different activity patterns. Activation of lateral pyramidal cells leads the activation of medial pyramidal cells. This occurs because geniculate afferents course from lateral to medial across the cortex and, thus, activate lateral pyramidal cells before they activate medial pyramidal cells. The transition from the initial depolarization to the primary propagating wave is smooth in the lateral pyramidal cells, while the activity pattern in medial pyramidal cells clearly shows the three components of the wave. The three populations of inhibitory interneurons have very different activity patterns. The majority of subpial cells are active during the initial depolarization (Fig. 5D). Activity in subpial cells falls to a low level by 200 ms and then increases slightly as the primary and secondary waves propagate across the cortex. The initial peak of subpial cell activity is driven by activity in the geniculate afferents. The tail of the activity is driven by recurrent collaterals of pyramidal cells, which become active as the waves

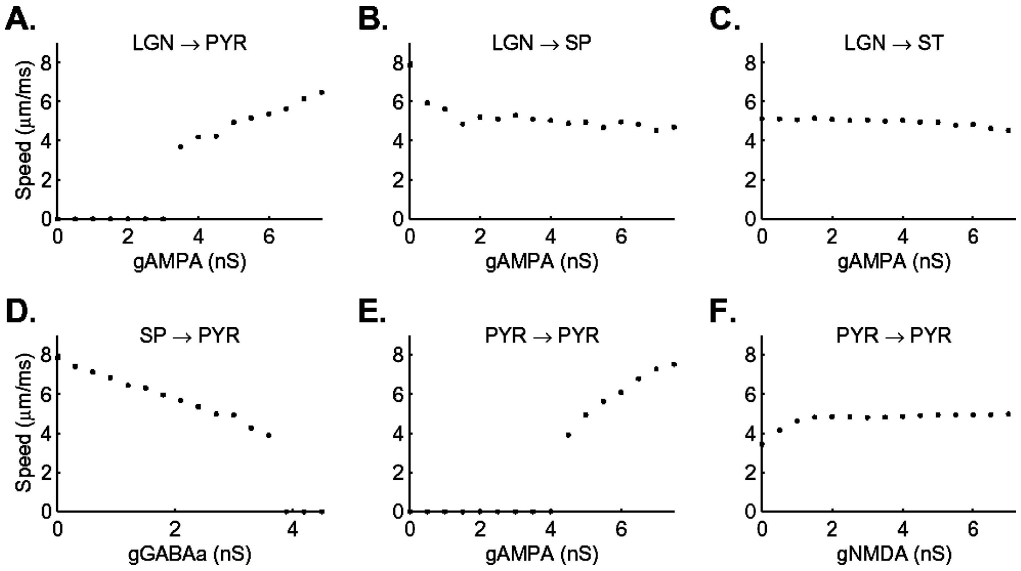

Figure 6. Effects of synaptic strength on wave formation and the speed of the primary propagating wave for synapses in the feedforward pathway. Each plot shows the speed of the simulated wave as a function of synaptic strength for one of the synapses in the feedforward pathway. Wave speeds of 0 μm/ms indicate that the stimulus produced an initial depolarization but did not produce a primary propagating wave. (A) Wave speed as a function of synaptic strength for synapses of geniculate afferents on pyramidal cells. (B) Wave speed as a function of synaptic strength for synapses of geniculate afferents on subpial cells. (C) Wave speed as a function of synaptic strength for synapses of geniculate afferents on stellate cells. (D) Wave speed as a function of synaptic strength for $GABA_A$ergic synapses of subpial cells on pyramidal cells. (E) Wave speed as a function of AMPAergic synapses of pyramidal cell collaterals on other pyramidal cells. (F) Wave speed of NMDAergic synapses of pyramidal cell collaterals on other pyramidal cells.

cross the cortex. The stellate cells fire only sporadically during the primary and secondary waves (Fig. 5E). The horizontal cells become active as the primary and secondary waves cross the cortex, driven by the activity of lateral and medial pyramidal cells (Fig. 5F). They remain active throughout the decay of the secondary wave.

The Feedforward Pathway Controls the Formation and Speed of Waves

The balance of excitation effected by geniculate afferents and inhibition effected by subpial cells on lateral pyramidal cells controls the formation and speed of primary waves. The effects of varying the conductance magnitudes of receptors in each of the synapses in the feedforward pathway are shown in Fig. 6. Individual plots in this figure show the speed of the primary propagating wave as a function of the maximal conductance density of specific receptor populations.

Geniculate Synapses on Pyramidal Cells. The synapses of geniculate afferents on pyramidal cells play a major role in controlling the formation and speed of cortical waves. Activation of pyramidal cells by geniculate afferents was required for the generation of initial depolarizations (Fig. 6A). There was no cortical response when the maximal density of AMPA receptors postsynaptic to geniculate afferents on pyramidal cells was 0 nS. Maximal densities of 0.5 nS–3.0 nS produced initial depolarizations that lasted between 198 and 250 ms but did not trigger propagating waves. The responses, then, had speeds of 0 μm/ms. The transition between an initial depolarization and a primary propagating wave is shown in Figs. 7D–F. Figure 7D shows the activity pattern of lateral pyramidal cells with a conductance density of 3.0 nS for geniculate synapses on lateral pyramidal cells. This conductance density is below the threshold for wave propagation. The stimulus produces a minor activation of lateral pyramidal cells that lasts less than 200 ms. Increasing the magnitude of the conductance density to 4.0 nS produced an initial depolarization that began dying out, but was sufficient to trigger a primary propagating wave (Fig. 7E). A conductance density of 7.0 nS produced an initial depolarization that continued smoothly into a primary propagating wave (Fig. 7F). This

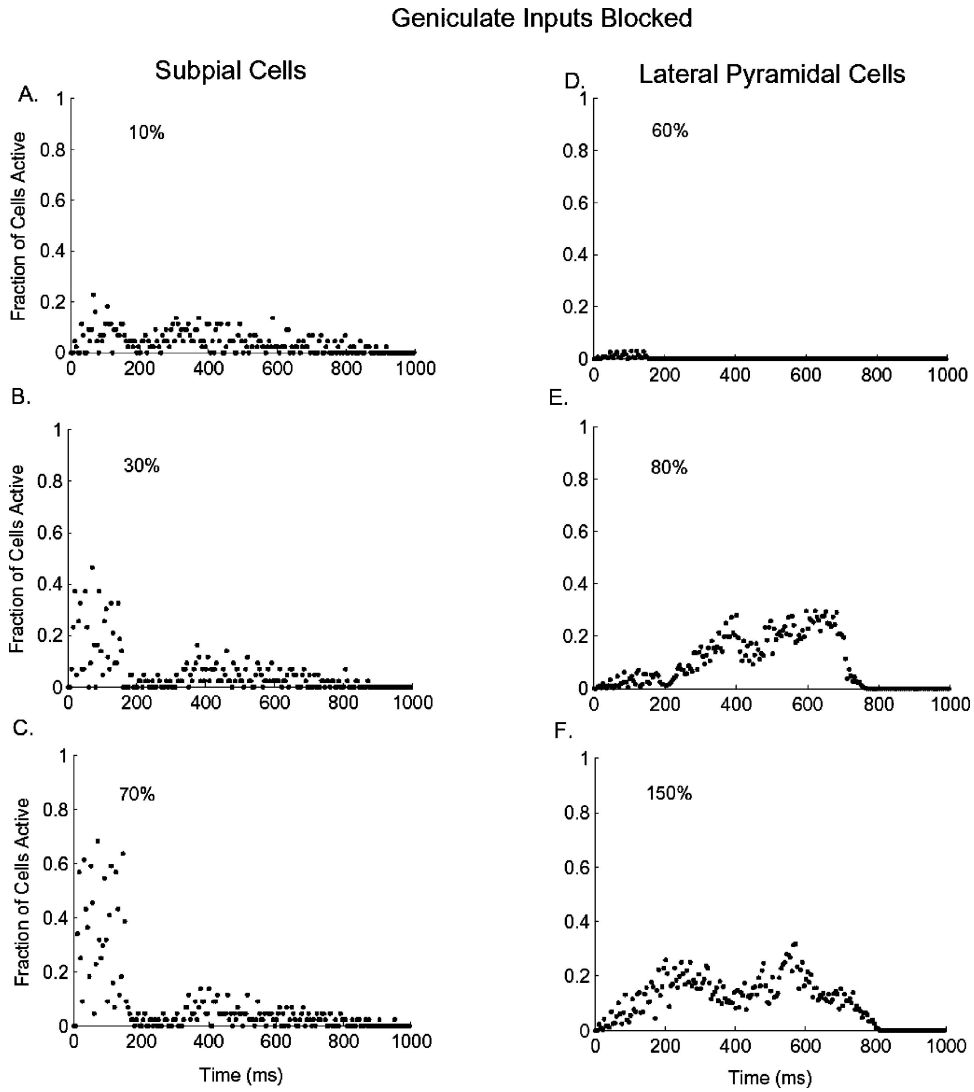

Figure 7. Activity patterns for subpial cells and lateral pyramidal cells as a function of the synaptic strength of geniculate synapses on subpial cells (left column) and geniculate synapses on lateral pyramidal cells (right column). Synaptic strengths for geniculate synapses on subpial cells are 10%, 30% and 70% of control values. Synaptic strengths for geniculate synapses on lateral pyramidal cells are 60%, 80% and 150% of control values.

behavior was typical for maximal densities of 3.5 nS–7.5 nS (Fig. 6A). The speed of the primary wave increased monotonically from 3.7 μm/ms to 6.5 μm/ms as the maximal density of AMPA receptors increased from 3.5 nS to 7.5 nS (Fig. 6A), and the fraction of active lateral pyramidal cells increased monotonically as a function of the maximal density of AMPA receptors (Fig. 8A).

Inhibition of pyramidal cells by subpial cells. The inhibitory effect of subpial cells on pyramidal cells involves two synapses, the excitatory synapses of geniculate afferents on subpial cells and the inhibitory synapses of subpial cells on pyramidal cells. Both primary and secondary waves occurred in the absence of an excitatory drive from geniculate afferents to subpial cells. The primary wave had a speed of 8.0 μm/ms (Fig. 6B). Increasing the maximal densities of AMPA receptors postsynaptic to geniculate afferents on subpial cells from 0 nS to 7.5 nS resulted in a monotonic decrease in the speed of the primary wave from 8.0 μm/ms to 4.7 μm/ms, but did not block the formation

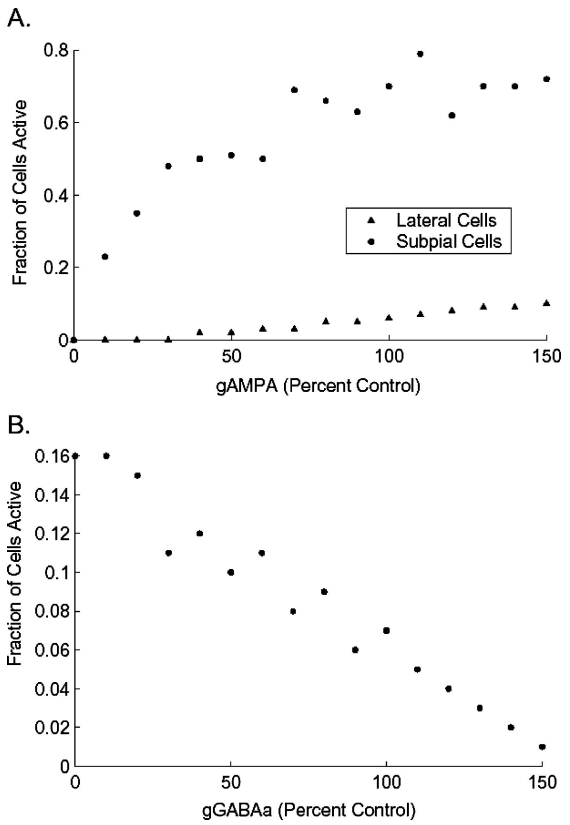

Figure 8. Fraction of active cells as a function of synaptic strengths. (A) Fraction of active lateral pyramidal cells (triangles) and subpial cells (circles) as a function of the synaptic strengths of geniculate afferents on lateral pyramidal cells and subpial cells. (B) Fraction of active lateral pyramidal cells as a function of the synaptic strength of $GABA_A$ergic synapses of subpial cells on lateral pyramidal cells.

of the wave. Increasing the maximal densities of AMPA receptors postsynaptic to geniculate afferents on subpial cells also resulted in a slow increase in the fraction of active subpial cells (8A). Examination of activity patterns (Fig. 7A–C) showed that increasing the conductance of AMPA receptors on subpial cells produced a rapid recruitment of subpial cells during the first 200 ms after stimulation. The fraction of subpial cells active during the first 200 ms after stimulus onset is a monotonically increasing function of the strength of the geniculate synapses. Subpial cell activity after 200 ms is due to excitatory drive from the pyramidal cells. It is present even if geniculate synapses on subpial cells are completely blocked because the synapses of geniculate afferents on pyramidal cells are intact.

In contrast to the synapses of geniculate afferents on subpial cells, the synapses of subpial cells on pyramidal cells can block wave formation. Varying the strength of subpial cell synapses on pyramidal cells between 0 nS and 3.6 nS produced a monotonic decrease in the speed of primary waves from 8.0 μm/ms to 4.0 μm/ms (Fig. 6D). Increasing synaptic strength above 3.6 nS blocked formation of the primary wave. Examination of the activity pattern of lateral pyramidal cells with the conductance density of $GABA_A$ receptors postsynaptic to subpial cell axons on lateral pyramidal cells at 3.5 nS, or below, showed initial depolarizations that triggered formation of primary and secondary waves (Fig. 9A and B). However, only initial depolarizations were produced when the maximal density of $GABA_A$ receptors was above 3.6 nS (Fig. 9C). The fraction of lateral pyramidal cells active was a monotonically decreasing function of the strength of $GABA_A$ergic synapses of subpial cells on lateral pyramidal cells (Fig. 8B). Changing the maximal density of $GABA_B$ receptors postsynaptic to subpial cells on pyramidal cells had little influence on wave speed. Wave speed changed from 5.0 μm/ms to 4.9 μm/ms when the maximal density was changed from 0 nS to 4.5 nS (not shown). Increasing the conductance density of $GABA_B$ receptors did not block formation of primary and secondary waves (Fig. 9D–F).

Differential Roles of Lateral and Medial Pyramidal Cells. The simulations just described indicate that the balance of excitation and inhibition on pyramidal cells determines whether or not an initial depolarization develops into a primary wave. However, the lateral and medial pyramidal cells play distinctly different roles in wave formation. Varying the maximal densities of AMPA receptors postsynaptic to geniculate afferents on only the pyramidal cells in D_L had the same effects on wave speed and duration as did varying the maximal densities of AMPA receptors on pyramidal cells in both D_L and D_M. Varying the maximal densities of AMPA receptors on pyramidal cells in D_M had no effect on the speed or duration of the waves. Similarly, varying the maximal conductance of $GABA_A$ receptors postsynaptic to subpial cells on only the lateral pyramidal cells in D_L had the same effects on wave speed and duration, as did changing the conductance on all pyramidal cells. Changing the maximal density of $GABA_A$ receptors on only the medial pyramidal cells in D_M had little effect on wave speed. Thus, the formation of primary waves is effected through pyramidal cells in D_L.

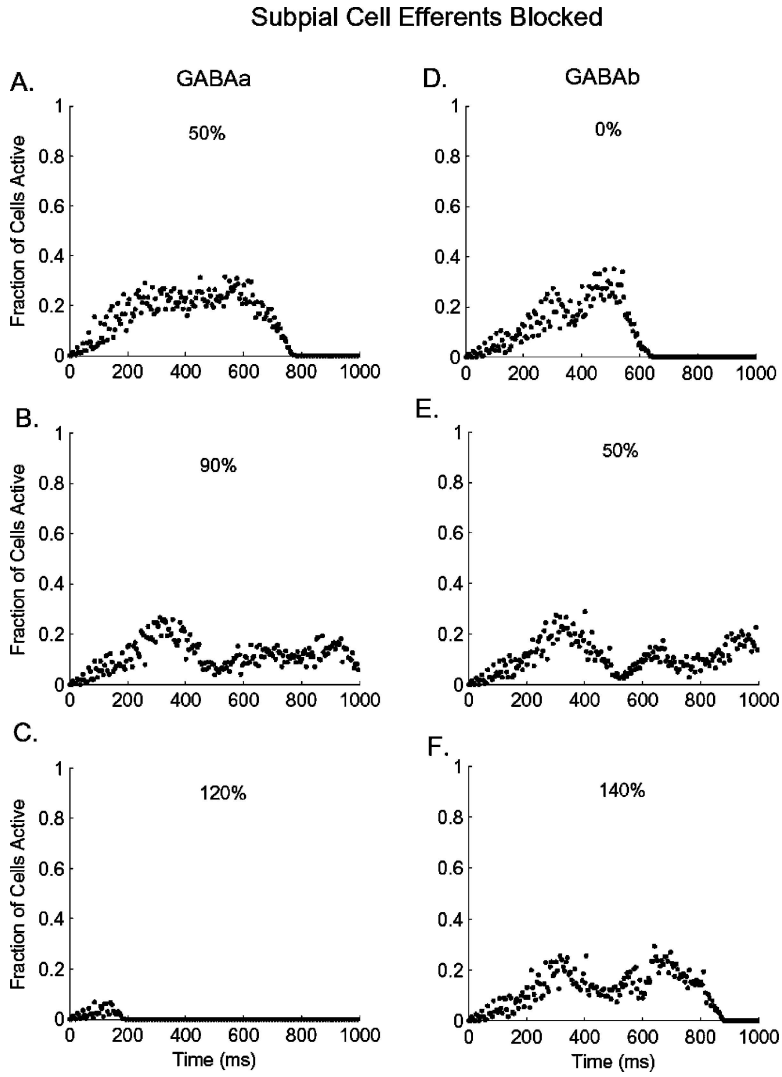

Figure 9. Activity patterns for pyramidal cells as a function of the synaptic strengths of subpial cell $GABA_A$ergic synapses (left column) and $GABA_B$ergic synapses (right column). Synaptic strengths for $GABA_A$ergic synapses are 50%, 90% and 120% of control values. Synaptic strengths for $GABA_B$ergic synapses are 0%, 50% and 140% of control values.

Pyramidal Cell Synapses on Other Pyramidal Cells Synapses are Required for Wave Propagation. Although the balance of excitation and inhibition effected on pyramidal cells by the geniculate and subpial afferents controls formation of primary waves, the excitatory interactions between pyramidal cells are necessary for propagation of the wave. Figure 10 shows the activity of subpial, lateral and medial pyramidal cells with all of the excitatory synapses of pyramidal cells blocked. Subpial cells showed their normal activity increase due to activation of geniculate afferents, but did not display the second phase of activity due to recurrent excitation from pyramidal cells. Lateral pyramidal cells showed only an initial depolarization, even though their level of activity is normally sufficient to trigger formation of a primary wave. Medial pyramidal cells were not activated. The AMPAergic and NMDAergic synapses of pyramidal cells on other pyramidal cells had different effects on wave formation and speed. The AMPAergic synapses of pyramidal cells on other pyramidal cells had major effects on the formation and speed of waves (Fig. 6E). Only initial depolarizations were produced when maximal densities of AMPA receptors postsynaptic to pyramidal cells on pyramidal

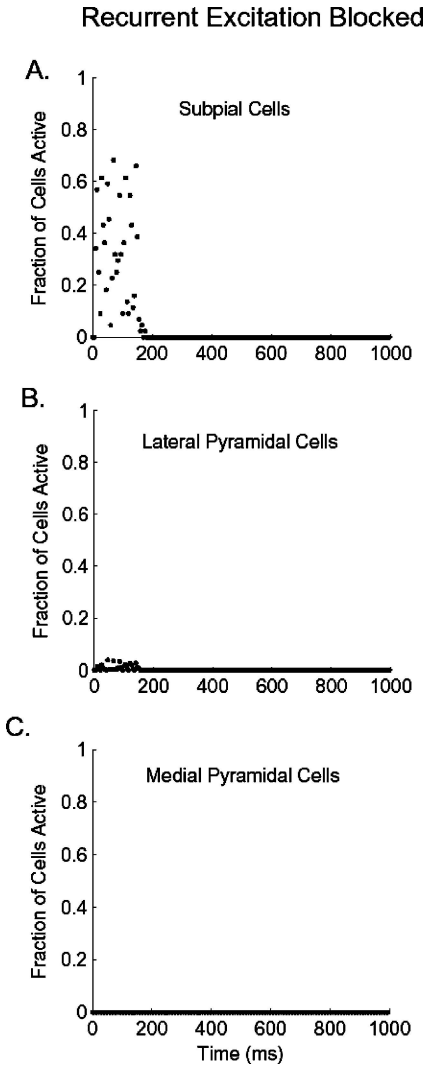

Figure 10. Activity patterns for subpial cells (A), lateral pyramidal cells (B) and medial pyramidal cells (C) with all recurrent synapses of pyramidal cell collaterals blocked.

cells were 0 nS–4.0 nS. The depolarizations had speeds of 0 μm/ms and lasted approximately 300 ms. Primary propagating waves with speeds that ranged from 3.9 μm/ms to 7.5 μm/ms were produced with densities of 4.5 nS–7.5 nS. Speed was a monotonic, increasing function of AMPA maximal density over the range of 4.5 nS–7.5 nS. By contrast, increasing the maximal density of NMDA receptors postsynaptic to pyramidal cell axons on other pyramidal cells had relatively minor effects on propagating waves (Fig. 6F). Both primary waves and secondary waves were formed when the maximal density of NMDA receptors postsynaptic to pyramidal cells on pyramidal cells was varied from 0 nS to 7.5 nS. A maximal density of 0 nS produced a primary wave with a speed of 3.4 μm/ms. Increasing the NMDA maximal density produced a slight increase in wave speed from 4.2 μm/ms to 4.9 μm/ms over the density range of 0.5 nS to 1.5 nS. Speeds were constant at 4.9 μm/ms at densities of 1.5 nS, and above.

The transition from an initial depolarization to a primary propagating wave is shown in a series of space-time plots (Fig. 11). Figure 11A shows the response of the model to a simulated light flash with the magnitude of the AMPA conductance postsynaptic to pyramidal cells on other pyramidal cells set to 4.0 nS. This conductance density is below the threshold for the transition to a primary propagating wave and subpial and lateral pyramidal cells produce only the bursts of activity due to geniculate activation. Figure 11B shows the response with the density set to 4.5 nS, which is just greater than the threshold for generation of a primary propagating wave. However, this level of activation is not sufficient to generate a secondary wave. Figures 11C and D show the responses obtained with conductance densities set at 5.0 nS and 7.5 nS, respectively. These plots show both primary and secondary propagating waves and a progressive decrease in the latency to production of the primary wave and an increase in the speed of the wave.

The Feedback Pathway Controls Wave Duration

Geniculate Input to Pyramidal Cells has Little Effect on Wave Duration. We have just seen that geniculate synapses control the formation of primary waves. However, they play little role in controlling the duration of waves once they have formed. The effects of synaptic strength on wave duration are illustrated in Fig. 12. Each graph in this figure is a plot of total wave duration (stars) and primary wave duration (dots) as a function of synaptic strength. Figure 12A shows wave duration as a function of the strength of geniculate synapses upon pyramidal cells. Synaptic strengths of 3.0 nS, and below, elicit an initial depolarization but not do not produce a primary propagating wave. The initial depolarizations last approximately 200 ms–250 ms. Synaptic strengths greater than 3.0 nS trigger a propagating wave with primary and secondary components. The durations of these waves decrease as the strength of geniculate synapses on pyramidal cells increases. However, this decrease is due to the progressive increase of inhibition in the

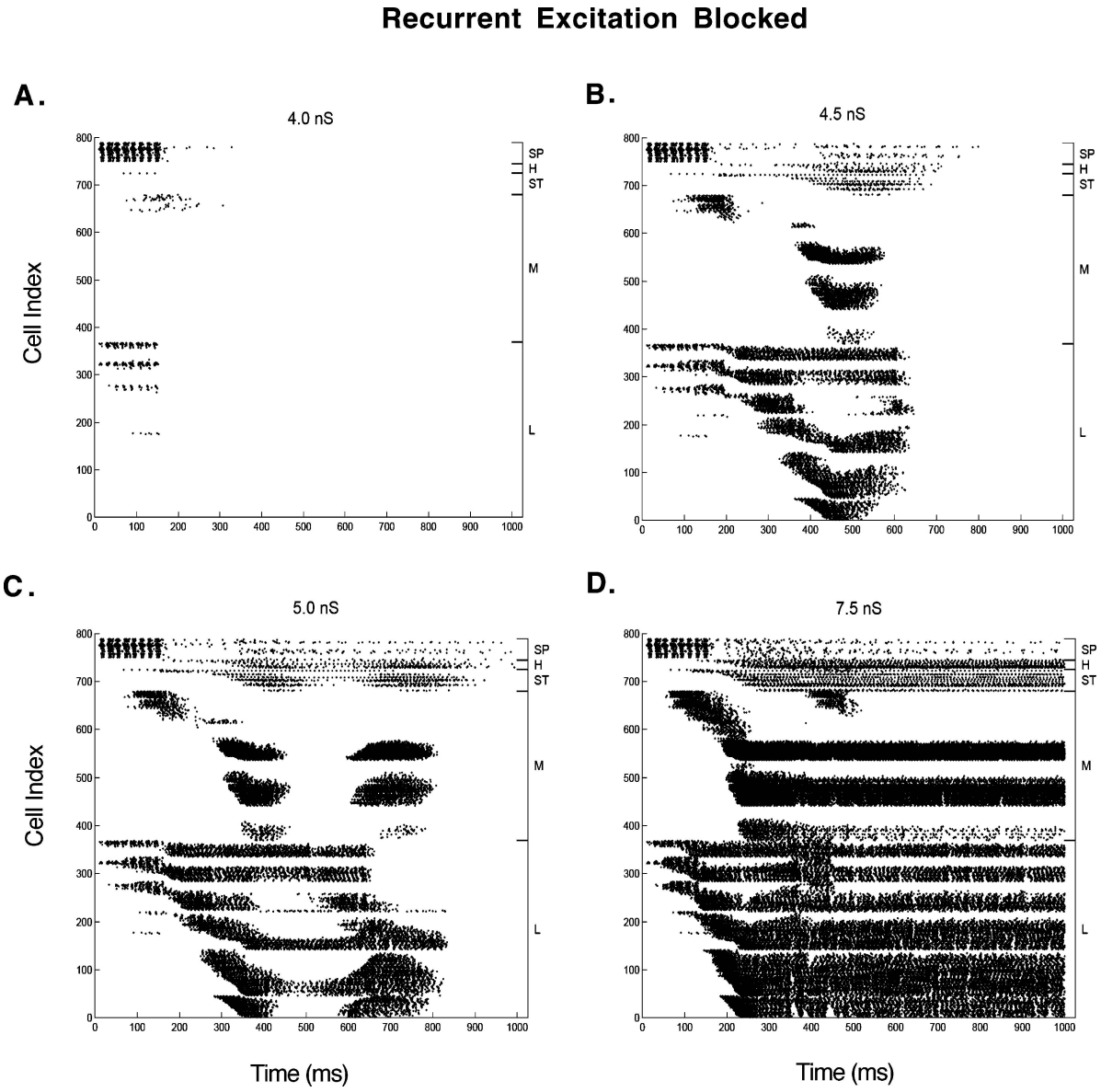

Figure 11. Space-time plot with recurrent excitation blocked. This is a space-time plot of the response of the model to a simulated 150 ms diffuse light flash with the strength of the of the AMPA receptor mediated recurrent excitation by pyramidal cell collaterals varied. (A) The synaptic strength is 4.0 nS. (B) The synaptic strength is 4.5 nS. (C) The strength is 5.0 nS. (D) The synaptic strength is 7.5 nS.

cortex due to increased excitatory drive by pyramidal cells collaterals. This can be seen in Fig. 12B, which shows wave duration as a function of the strength of geniculate synapses on pyramidal cells with all inhibition in the cortex blocked.

Subpial Cells have Little Effect on Wave Duration. Total wave duration and the duration of primary waves were approximately constant as the strength of $GABA_A$ergic synapses of subpial cells on pyramidal cells was varied from 0 nS to 3.6 nS (Fig. 12D). Synaptic strengths above 3.6 nS blocked the formation of the primary wave and produced only initial depolarizations. Varying the strength of the AMPAergic synapses of pyramidal cell collaterals on subpial cells had no consistent effect on total wave durations.

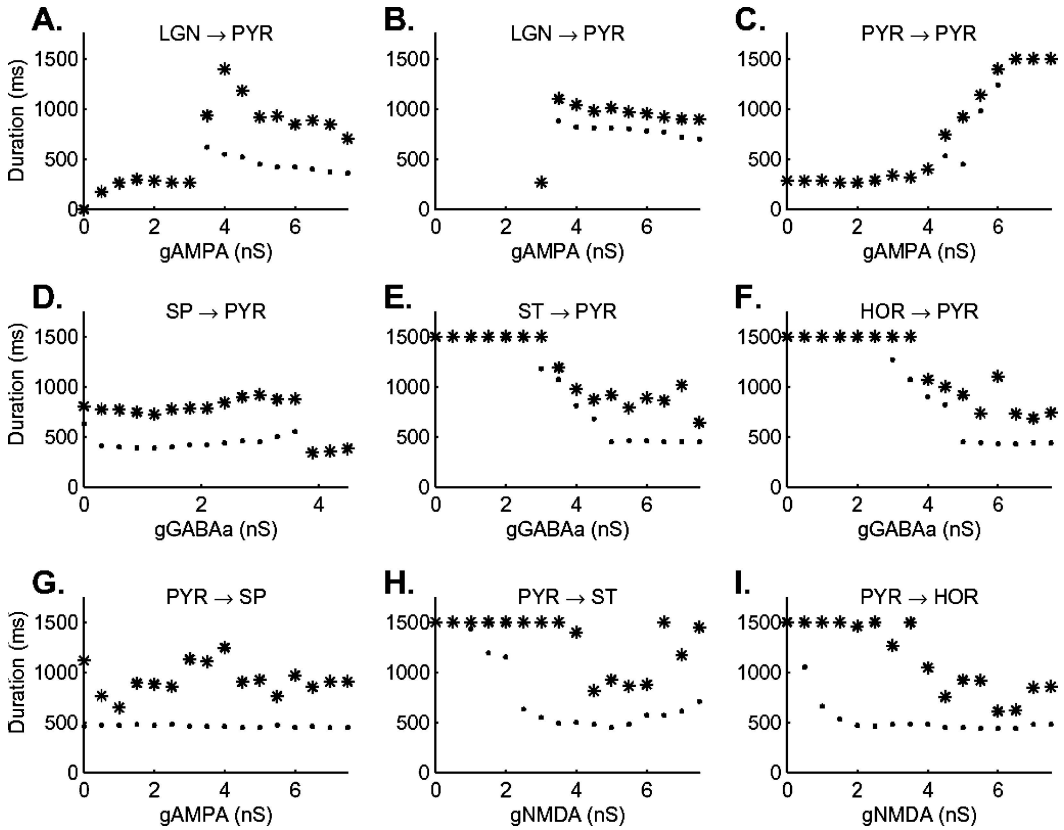

Figure 12. Effects of synaptic strength on wave duration. Each graph is a plot of the total duration of the wave (stars) and the duration of the primary propagating wave (dots) as a function of the maximal conductance density of a specific population of synapses. Dots and stars overlap for some conductance values. The duration of the secondary wave can be obtained by subtracting the duration of the primary propagating wave from the duration of the total wave. (A) Effect of varying the strength of the AMPAergic synapses of geniculate neurons on pyramidal cells. (B) Effect of varying the strength of the AMPAergic synapses of geniculate neurons on pyramidal cells with all inhibitions in the cortex model blocked. (C) Effect of varying the strength of the AMPAergic synapses of pyramidal cell collaterals on other pyramidal cells. (D) Effect of varying the strength of the $GABA_A$ergic synapses of subpial cells on pyramidal cells. (E) Effect of varying the strength of the $GABA_A$ergic synapses of stellate cells on pyramidal cells. (F) Effect of varying the strength of the $GABA_A$ergic synapses of horizontal cells on pyramidal cells. (G) Effect of varying the strength of the AMPAergic synapses of pyramidal cell collaterals on subpial cells. (H) Effect of varying the strength of the NMDAergic synapses of pyramidal cells on stellate cells. (I) Effect of varying the strength of the NMDAergic synapses of pyramidal cells on horizontal cells.

The durations of primary propagating waves were constant (Fig. 12G). The activity pattern for subpial cells (Figs. 5D and 15D) shows that subpial cells are active throughout the duration of the wave. However, it appears that a sufficient number of subpial cells are not active during the primary and secondary waves to have a significant direct effect on pyramidal cell activity.

Stellate Cells have Major Effects on Wave Duration. Since stellate cells are postsynaptic to geniculate afferents, they could be considered as elements in the feedforward pathway. However, the synapses of geniculate afferents on stellate cells had little effect on wave dynamics. Increasing the maximal density of AMPA receptors postsynaptic to geniculate afferents on stellate cells caused a slight, monotonic decrease in the speed of the primary wave from 5.1 μm/ms to 4.5 μm/ms (Fig. 6C). The duration of the primary wave was approximately constant at 500 μm/ms as the strength of the geniculate synapses on stellate cells was varied (not shown). The total duration of the wave was variable, but showed no systematic increase or decrease. The stellate cells are, consequently, not functional components of the feedforward pathway.

However, stellate cells are also contacted by pyramidal cell axons and are, consequently, potential elements

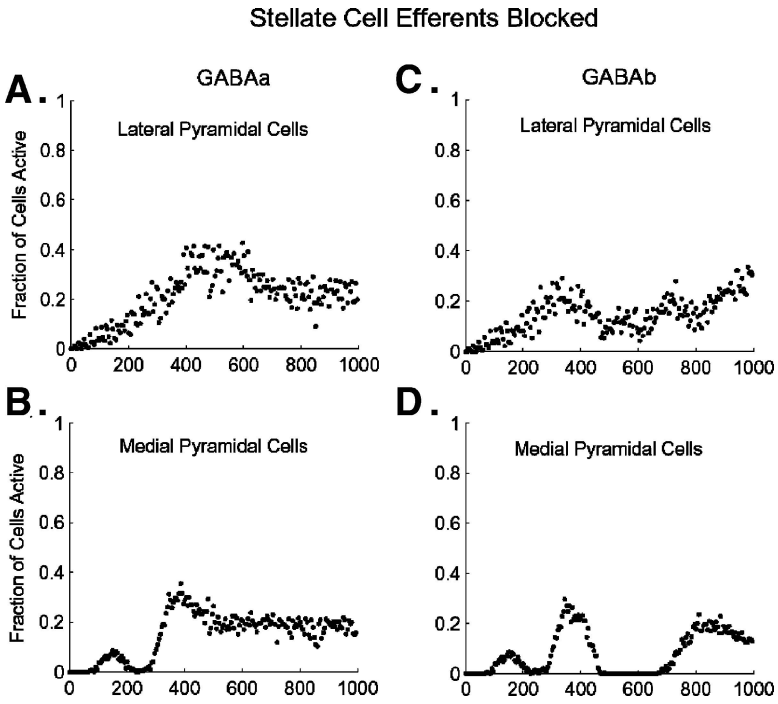

Figure 13. Effects of $GABA_A$ergic and $GABA_B$ergic synapses of stellate cells on lateral pyramidal and medial pyramidal cells. The plots show the activity patterns of lateral pyramidal cells (A, C) and medial pyramidal cells (B, D) with the $GABA_A$ergic (left column) and the $GABA_B$ergic (right column) synapses of stellate cells blocked.

in the feedback pathway. Consistent with this interpretation, the duration of primary waves was 1,500 ms when the maximal density of $GABA_A$ receptors postsynaptic to stellate cells on pyramidal cells was lower than 2.5 nS (Fig. 12E). It decreased monotonically from 1,500 ms to 450 ms when the maximal density increased from 2.5 nS to 5.0 nS, and remained constant at about 450 ms with higher densities. Total durations were 1,500 ms when the maximal density of $GABA_A$ receptors was lower than 3.0 nS, and decreased to 645 ms when the maximal density increased from 3.5 nS to 7.5 nS. Activity patterns for lateral and medial pyramidal cells with $GABA_A$ergic or $GABA_B$ergic synapses blocked show that both subtypes of GABA receptors particicipate in the control of wave duration (Fig. 13). Blocking $GABA_A$ergic or $GABA_B$ergic synapses of stellate cells on either lateral (Fig. 13A, C) or medial (Fig. 13B, D) pyramidal cells prolongs activity in the two populations of pyramidal cells. Varying the maximal density of NMDA receptors postsynaptic to pyramidal cells on stellate cells also had a significant effect on wave duration (Fig. 12H). Primary wave duration was constant at 1,500 ms as the density of NMDA receptors postsynaptic to pyramidal cells axons varied from 0 nS to 1.0 nS. It decreased monotonically to about 500 ms as the receptor density was increased from 1.5 nS to 5.0 nS, and then increased slightly as the receptor density was increased to 7.5 nS. Similarly, total wave durations were 1,500 ms for receptor densities ranging from 0 nS to 3.5 nS, but gradually decreased to 815 ms over the density range of 4.5 nS to 6.0 nS.

Horizontal Cells have Major Effects on Wave Duration. Horizontal cell inhibition of lateral and medial pyramidal cells had differential effects on wave duration. Primary wave duration decreased from 1,500 ms to 440 ms as $GABA_A$ receptor density increased over the range of 2.5 nS to 7.5 nS for horizontal cell axons contacting pyramidal cells (Fig. 12F). Total wave durations decreased from 1,500 ms to 740 ms. Primary wave duration decreased from 900 ms to 450 ms over the range of 0.5 nS to 7.5 nS for horizontal cell axons contacting medial pyramidal cells. Total wave duration varied between 1,000 ms to 800 ms, but no clear trend was present. Figure 14 shows activity patterns for lateral and medial pyramidal cells with the $GABA_A$ergic synapses of horizontal cells blocked.

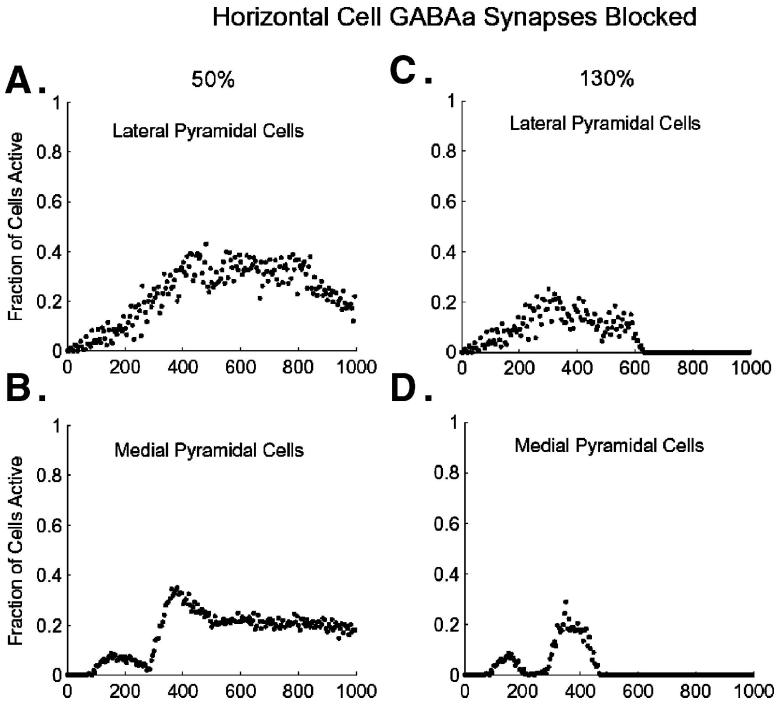

Figure 14. Effects of $GABA_A$ergic and synapses of horizontal cells on lateral pyramidal and medial pyramidal cells. The plots show the activity patterns of lateral pyramidal cells (A, C) and medial pyramidal cells (B, D) with the $GABA_A$ergic blocked 50% (left column) and 130% (right column).

Varying the strength of the $GABA_A$ergic synapses of horizontal cells on lateral (Fig. 14A, C) or medial (Fig. 14B, D) pyramidal cells controls the fraction of pyramidal cells active during the secondary wave. In particular, inhibition of pyramidal cells by horizontal cells can block the formation of the secondary wave. The synapses of pyramidal cells on horizontal cells had major effects on wave duration (Fig. 12I). The duration of primary waves decreased monotonically from 1,500 ms to 470 ms when the maximal density of NMDA receptors postsynaptic to pyramidal cell axons on horizontal cells was increased from 0 nS to 2.0 nS, and then varied slightly between 450 ms and 480 ms when the maximal density increased above 2.0 nS. Total wave duration was 1,500 ms when the maximal density of NMDA receptors was lower than 2.0 nS, and decreased monotonically from 1,500 ms to 610 ms when the maximal density was increased above 2.0 nS. Varying the density of NMDA receptors on lateral and medial pyramidal cells separately had some effect on wave duration, but varying NMDA receptor density on both sets of pyramidal cell synapses simultaneously had a greater effect than did varying the density on either population alone (not shown).

Pyramidal Cell Collaterals Effect Wave Duration. Total wave duration was approximately constant at about 800 ms as the maximal density of NMDA receptors postsynaptic to pyramidal cell axons on other pyramidal cells was varied. By contrast, the durations of both primary and secondary waves increased as the maximal density of AMPA receptors postsynaptic to pyramidal cell afferents on other pyramidal cells was increased above 4.0 nS (Fig. 12C). The duration of the primary wave increased approximately linearly from about 450 ms at 4.5 nS to 1,500 ms for densities of 6.5 nS and greater. The total duration of the wave increased linearly from about 750 ms at 4.5 nS to 1,500 ms at densities of 6.5 nS, and greater. However, the duration of the primary wave decreased slightly from 500 ms to 460 ms over the density range from 0.5 nS to 1.5 nS, apparently due to an increased excitatory drive to inhibitory neurons, and then remained approximately constant at 450 ms for densities of 2.0 nS and greater.

Interactions Between Populations of Inhibitory Interneurons Affects Wave Duration. Although subpial cells are considered as elements of the feedforward

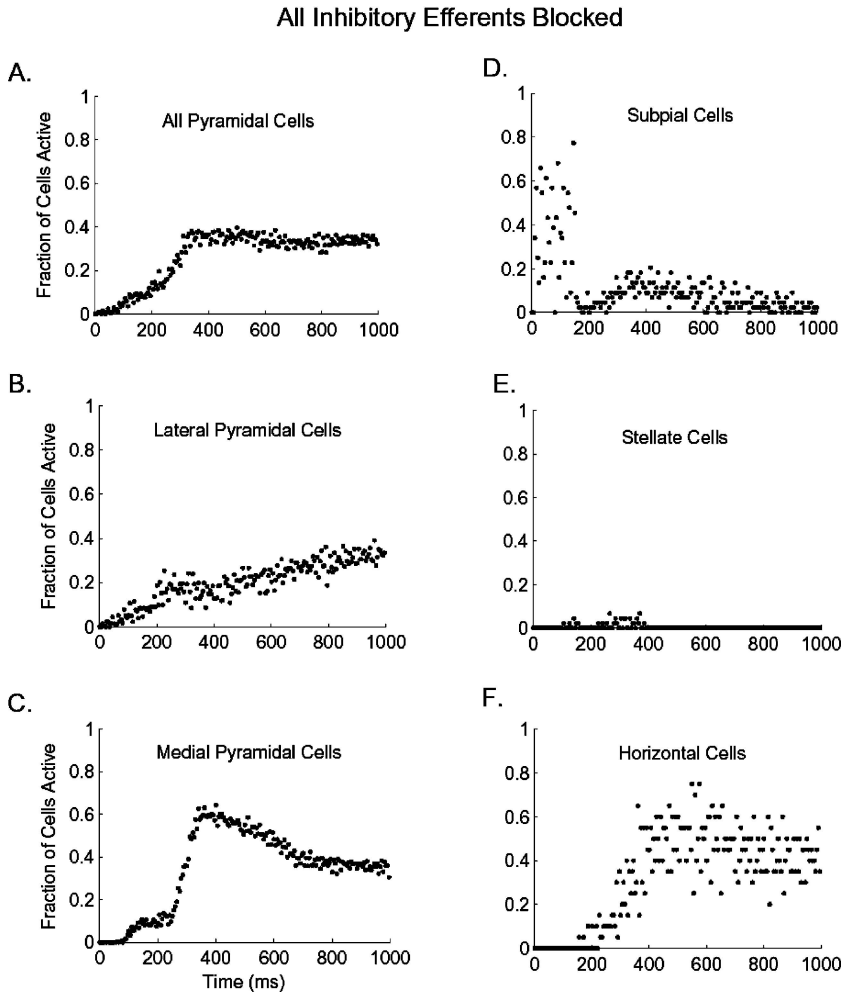

Figure 15. Activity pattern of cortical neurons with all inhibition blocked. Plots of the activity of all pyramidal cells, (A) lateral pyramidal cells, (B) medial pyramidal cells, (C) subpial cells, (D) stellate cells (E) and horizontal cells (F) as a function of time with all inhibitory synapses in the model blocked.

pathway and have their major role in controlling wave formation and speed, they also have an indirect effect on the inhibitory cells in the feedback pathway. The duration of primary waves decreased monotonically from 630 ms to 390 ms when the maximal density of $GABA_A$ receptors postsynaptic to subpial cells on pyramidal cells increased from 0 nS to 1.2 nS. The duration then increased from 390 ms to 550 ms monotonically when the maximal density increased from 1.2 nS to 3.6 nS. The total duration of waves decreased monotonically from 805 ms to 725 ms when the maximal density increased to 1.2 nS and increased up to 920 ms when the maximal density increased above 1.2 nS. These effects result from the decreased drive of pyramidal cells to stellate and horizontal cells caused by the inhibition of pyramidal cells by subpial cells. Thus, varying the maximal densities of AMPA receptors postsynaptic to geniculate afferents on pyramidal cells, with the excitation on subpial cells blocked, increased the duration of the primary wave and the total wave duration (Fig. 12B). Blocking pyramidal cell excitation on stellate cells, on horizontal cells, or both, produced primary waves with durations of 1,500 ms and total wave durations of 1,500 ms. Increasing the excitatory drive to pyramidal cells from geniculate afferents resulted in an increased excitatory drive to the three populations of inhibitory interneurons, which feed back on the pyramidal cells, reducing their firing level and decreasing wave duration.

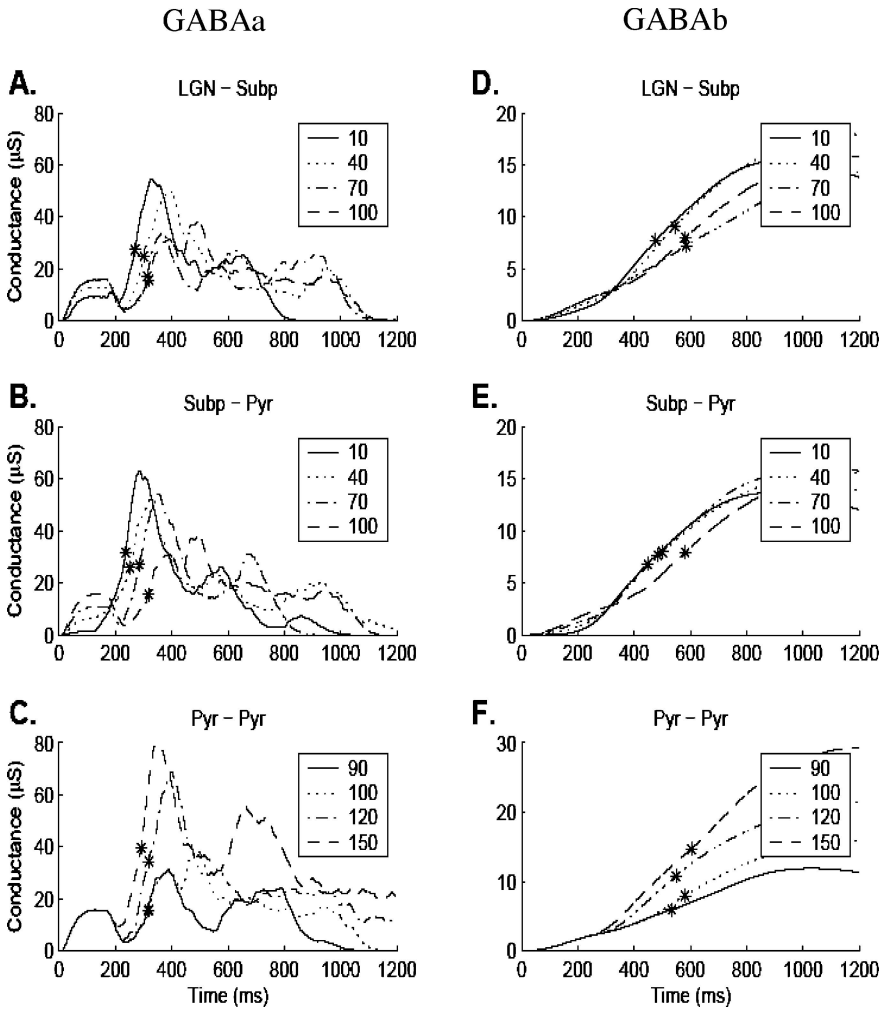

Figure 16. Total inhibitory conductances on pyramidal cells. Plots in this figure show the time courses of the total $GABA_A$ (left column) and the total $GABA_B$ (right column) conductances on 184 pyramidal cells in the rostral corner of the cortex. Plots in the top row show the effect of varying the strength of geniculate synapses upon subpial cells. Plots in the middle row show the effect of altering the strengths of subpial cell synapses upon pyramidal cells. Plots in bottom row show the effect of altering the strengths of pyramidal cell synapses upon other pyramidal cells.

Global Perspective on Inhibition

The preceding simulations have examined the effects of specific receptor types on the activation of specific populations of cells. They suggest that the feedforward and feedback pathways play specific roles. However, an individual population of cortical cells can be influenced by several populations of inhibitory cells and by both $GABA_A$ and $GABA_B$ receptor-mediated inhibition. The overall effects of inhibition in the cortex are shown explicitly in Fig. 15, which shows the activity pattern of each population of cortical cells with all inhibitory synapses blocked. The activity of all pyramidal cells increased steadily through an initial depolarization, formed a primary wave and then reached a steady state of slightly less than 40% of pyramidal cells active at about 350 ms after stimulation (Fig. 15A). Lateral and medial pyramidal cells showed different activity patterns. Lateral pyramidal cell activity increased steadily from the initial depolarization to the steady state level, which it reached by about 1,300 ms after stimulation (Fig. 15B). By contrast, the activity of medial pyramidal cells reached a peak of about 60% by about 350 ms and then decreased to the steady

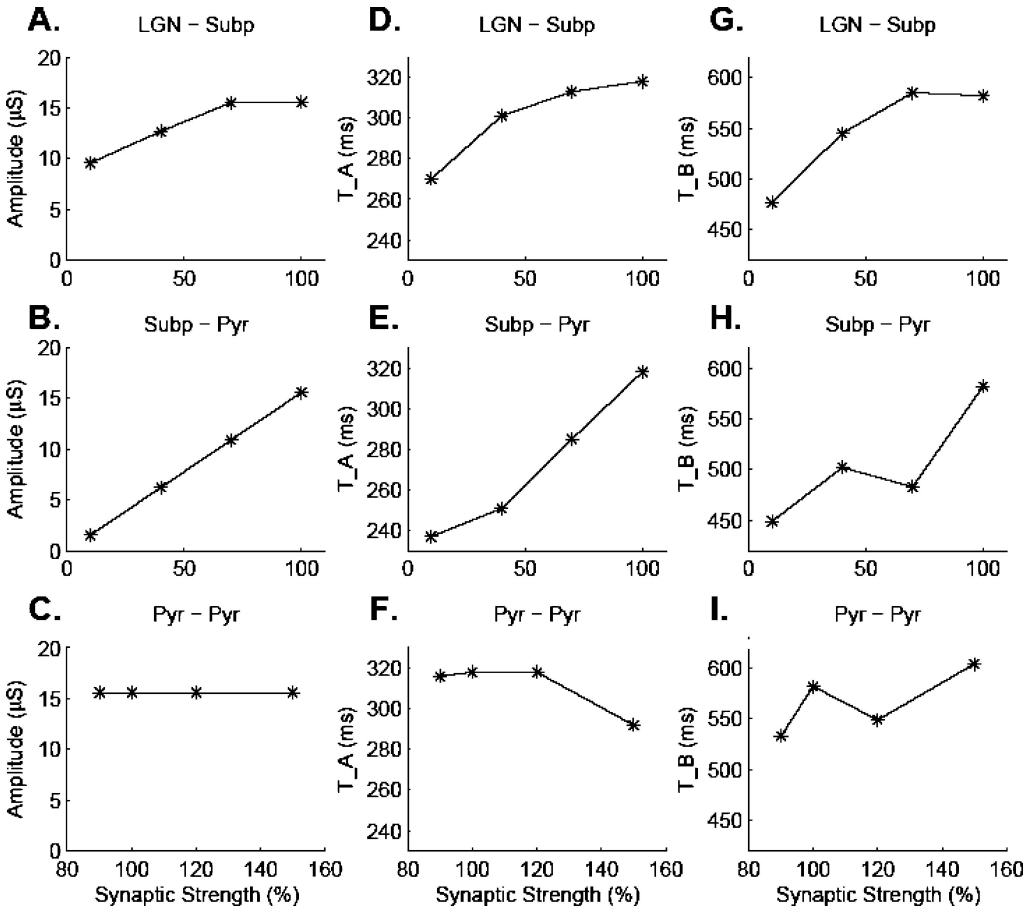

Figure 17. Parameters of total inhibitory conductances as a function of synaptic strength. The maximal amplitude of the $GABA_A$ergic conductance in the first 250 ms (left column), the amplitudes 50% rise times of $GABA_A$ conductances (TA, center column) and 50% rise times of $GABA_B$ conductances (TB, right column) are plotted as a function of synaptic strength. Plots in the top row show the effects of altering the strengths of geniculate synapses upon subpial cells. Plots in the middle row show the effects of altering the strengths of subpial cell synapses upon pyramidal cells. Plots in the bottom row show the effects of altering the strengths of pyramidal cell synapses upon pyramidal cells.

state level by about 800 ms (Fig. 15C). The activity patterns of the three populations of inhibitory cells were quite different. Subpial cells showed their characteristic two activity phases, but a larger fraction of subpial cells were active throughout the second phase (Fig. 15D), as compared to the control case (Fig. 5B). Stellate cells showed their characteristic, low level of activity throughout the duration of the primary wave (Fig. 15E). Horizontal cells began a linear increase in activity from about 250 ms to a peak of about 70% at around 600 ms, and then decreased to a mean steady state level of about 40% (Fig. 15F).

The differential contribution of $GABA_A$ and $GABA_B$ receptor are illustrated in Figs. 16 and 17. Figure 16 shows plots of the total $GABA_A$ receptor-mediated conductance (left column) and the total $GABA_B$ receptor-mediated conductance (right column) as measured in 184 pyramidal cells situated in the rostral lateral corner of the cortex. This region was chosen for analysis because it is the site at which the cortical wave is generated. The total $GABA_A$ conductance and the total $GABA_B$ conductance was calculated for each cell and the individual $GABA_A$ and $GABA_B$ conductance time series were summed. The summed responses were passed through a second order low pass filter ($1/(s^2 + 2s\tau^{-1} + \tau^{-2})$, $\tau = 20$ ms) to produce smooth traces. The individual plots show the effects of varying the strength of the AMPAergic synapses of geniculate afferents on subpial cells (top row), the GABAergic synapses of subpial cells

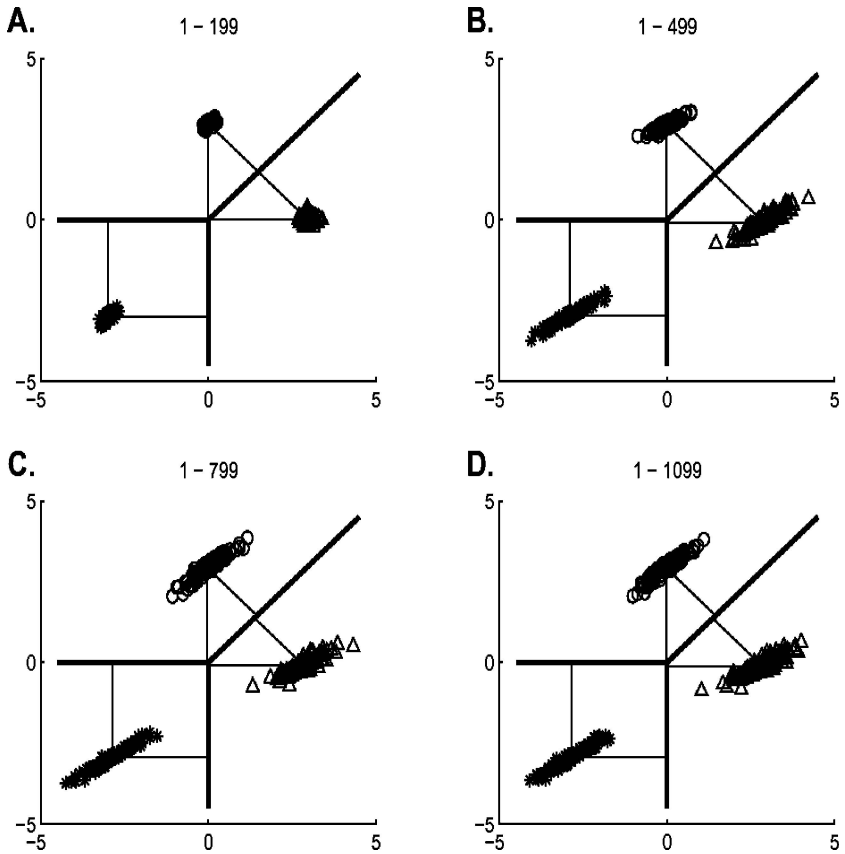

Figure 18. Discrimination plots for spot stimuli presented at the left, center and right of the geniculate complex. Plots show points in decision space generated by presenting each stimulus 100 times in the presence of noise. Lines from clusters of points to boundary lines are measures of discriminability. Individual plots correspond to expanding time windows of different lengths.

on pyramidal cells (middle row) and the AMPAergic synapses of pyramidal cells on other pyramidal cells (bottom row). The traces in the left column indicate that the $GABA_A$ergic conductance shows an initial burst of activity in the first 250 ms after the stimulus that can be attributed to activity in the subpial cells. Figure 17 (left column) shows plots of the maximal amplitude of the $GABA_A$ergic conductance within the initial burst period as a function of the synaptic strength. The plots indicate that the synapses of subpial cells on pyramidal cells have the strongest effect on the magnitude of this early conductance (Figs. 16B, 17B), the synapses of the geniculate afferents on the subpial cells have a moderate effect (Figs. 16A, 17A), and the synapses of pyramidal cells collaterals have no effect (Figs. 16C, 17C). The early $GABA_A$ conductance is followed by two conductance peaks that occur during the primary and secondary waves. Altering synaptic strength modulates the amplitudes of these peaks and shifts their onsets. The latency of the peaks was quantified by measuring the time at which each peak reaches its half-maximal amplitude (TA). The plots in Fig. 17 (Fig. 17D–F) show that geniculate synapses on subpial cells, subpial synapses on pyramidal cells and pyramidal cell synapses on pyramidal cells all alter TA. The plots in the right column of Fig. 16 show the time courses of the $GABA_B$ receptor-mediated conductance in pyramidal cells. All of the plots show low amplitude $GABA_B$ conductances during the first 250 ms. The conductances subsequently increase to a maximal value near 1000 ms. Altering the strengths of the synapses modulates the maximal amplitudes (Fig. 16D–F) and times to half maximal amplitudes (TB) of the conductances (Fig. 17G–I). The simulations indicate that the primary wave is controlled principally by $GABA_A$ergic conductances. A point that is not obvious from the activity plots for the three populations of inhibitory cells is that the amplitude of the early conductance is much

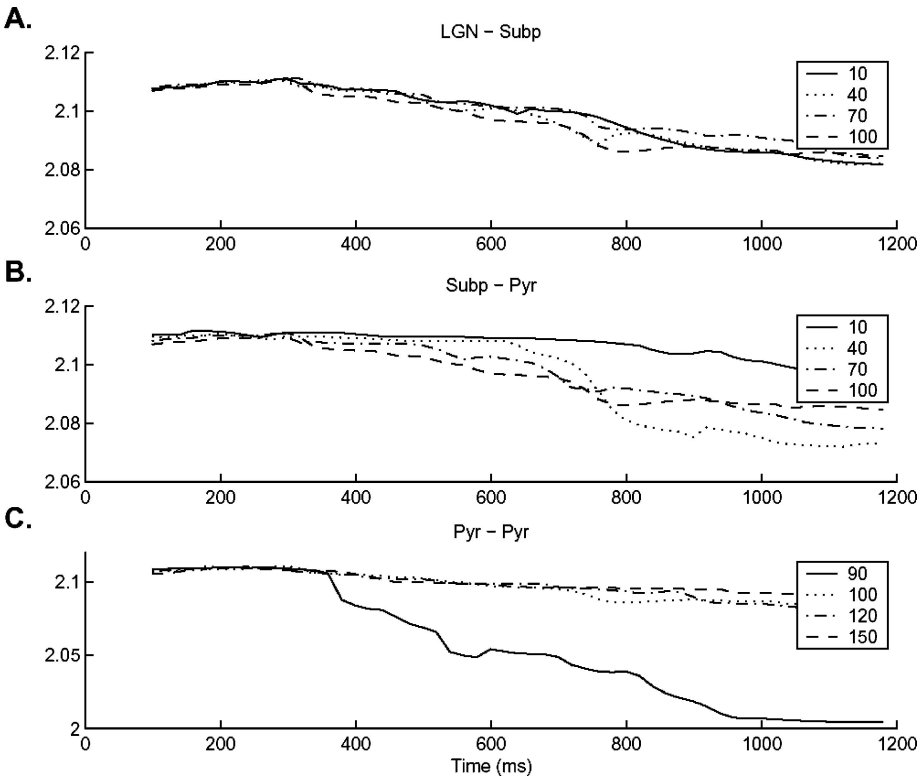

Figure 19. Detection distances as functions of time. Plot (A) shows the effect of varying the strength of geniculate synapses on subpial cells on detection distances. Plot (B) shows the effect of varying the strength of subpial cell synapses on pyramidal cells on detection distances. Plot (C) shows the effect of varying the strength of pyramidal cell synapses on pyramidal cells on detection distances.

smaller than the amplitude of the middle conductance, even given the strong peak of subpial cell activity. The relatively low level of subpial and stellate cell activity between 250 and 600 ms produces a surprisingly strong GABA conductance. Pyramidal cell activity during the secondary wave is controlled principally by $GABA_B$ conductances.

Encoding Properties of Waves

Nenadic et al. (2001) and Du et al. (2005) found that cortical waves contain information about the position and speed of objects in visual space. We studied the relationship between the strength of synaptic interactions between populations of cortical neurons and the detectability of spots of light by activating groups of geniculate neurons positioned at the left, center and right of the geniculate complex. There were 100 simulations of each cluster of neurons. Responses were analyzed by a double KL decomposition using an expanding detection window. Figure 18 shows the positions of the resulting points in decision space plotted for four different time windows. The plots indicate that the three points can be easily discriminated from each other for all four time windows. The plots in Fig. 19 show the minimum detection distance between a cluster and the boundary between two detection regions. Relatively large detection distances indicate that two clusters are easily discriminable. Individual plots show the effect on minimum detection distances by varying the strength of the geniculate synapses on subpial cells (Fig. 19A), subpial cell synapses on pyramidal cells (Fig. 19B) and pyramidal cell synapses on pyramidal cells (Fig. 19C). The plots indicate that varying synaptic strengths has essentially no effect on detectability for time windows of up to 400 ms. Detection distances begin to decrease, but very little, after 400 ms. This indicates the robustness of detectability of the turtle visual cortex model.

Discussion

Components of Cortical Waves

The cortical waves simulated in our large-scale model of turtle visual cortex were divided into three components for the purpose of analysis in this study. Each component occurs in real cortices. The first component, an initial depolarization, always occurs at the rostral pole of the cortical model. Voltage sensitive dye studies demonstrate that responses in the real turtle visual cortex also begin as a depolarization that is localized to the rostral pole of the visual cortex and last for approximately 150 ms following a retinal flash (Senseman, 1999). Initial depolarizations have been reported in the somatosensory cortex of rats following mechanical stimulation of whiskers using voltage sensitive dyes. Petersen and Sakmann (2001) found that electrical stimulation of a layer 4 barrel *in vitro* evoked an excitatory response limited to the stimulated barrel-column. Minimal deflection of a whisker *in vivo* resulted in a response restricted to the corresponding barrel in somatosensory cortex (Petersen et al., 2003). Golomb and Amitai (1997) found that electrical stimulation of slices of rat neocortex resulted in a restricted depolarization when sufficiently high levels of the non-NMDA receptor antagonist, CNQX, were included in the bath solution.

When the ratio of excitatory to inhibitory conductances is low, the initial depolarization dies out and does not develop to propagating waves. Higher ratios of excitatory to inhibitory conductances result in primary propagating waves in the model cortex. Similar waves have been reported in the visual cortex of turtles using both multielectrode arrays and voltage sensitive dye methods (Prechtl et al., 1999, 2000; Senseman, 1999). As in the model cortex, these dyes originate near the rostral pole of the visual cortex and propagate anisotropically across the cortex. Propagating waves have now been reported in mammals in the visual cortex (Grinvald et al., 1994; Bringuier et al., 1999; Contreras and Llinás, 2001), somatosensory cortex (Kleinfeld and Delaney, 1996; Ghanzafar and Nicoleilis, 1999; Contreras and Llinás, 2001; Petersen et al., 2003; Derdikman et al., 2003), frontal cortex (Seidemann et al., 2002) and hippocampus (Traub et al., 1991). In turtle visual cortex, the waves propagate along the rostral-caudal axis of the cortex in both the model (Nenadic et al., 2003; Wang, 2006) and the real (Senseman, 1999; Senseman and Robbins, 1999, 2002) cortex. The pattern of wave propagation is similar in the barrel cortex of rats in that waves propagate predominantly along the rows of barrels (Kleinfeld and Delaney, 1996; Petersen et al., 2003; Derdikman et al., 2003).

A secondary wave, or reflection, occurs when the primary propagating wave reaches the caudal pole of the cortex model in many, but not all, cases. Secondary waves occur in turtle cortices following flash stimuli presented to the retina (Senseman, 1999). Reflection of waves is also seen within slices of rat neocortex (Chagnac-Amitai and Connors, 1989; Chervin et al., 1988).

Feedforward and Feedback Pathways

Feedforward and feedback pathways can be recognized in turtle visual cortex based on the anatomical relationship of geniculate and pyramidal cell afferents to different populations of cells. Geniculate afferents run in a fascicle from lateral to medial across visual cortex (Heller and Ulinski, 1986; Mulligan and Ulinski, 1990). Visual cortex corresponds to the cytoarchitectonic area, D, which is divided into two cytoarchitectonically distinct subcomponents, D_{L} and D_{M} (Colombe and Ulinski, 1999). The two subcomponents of D contain pyramidal cells that differ morphologically. Lateral pyramidal cells have well formed basal and apical dendrites while medial pyramidal cells have reduced basal dendrites. The somata of lateral pyramidal cells participate in large clusters of neurons with touching somata while medial pyramidal cells are isolated from their neighbors or participate in small clusters of neurons. Geniculate afferents inersect the proximal dendrites and somata of lateral pyramidal cells. They enter the cortex through a relatively restricted region of D_{L} that is situated near the rostral pole of the cortex. This is presumably because the density of geniculate synapses on lateral pyramidal cells in the rostral cortex is much higher than the density of geniculate synapses on medial or lateral pyramidal cells in the caudal cortex. Subpial cells have their somata and dendrites embedded in the fascicle of geniculate afferents that courses across the cortex (Colombe et al., 2004). Stellate cells have dendrites that extend into the band of geniculate afferents. Both subpial and stellate cells have axons that intersect the dendrites of pyramidal cells. Thus, lateral pyramidal, subpial and stellate cells can be considered in a feedforward pathway

with both excitatory and inhibitory limbs. Both lateral and medial pyramidal cells give rise to corticofugal efferents (Ulinski, 1986), but they also have collaterals that arborize within *D*. The collaterals contact other pyramidal cells, and intersect subpial, stellate and horizontal cells. Neurons in each of the three inhibitory populations can, consequently, be regarded as elements in a feedback pathway onto pyramidal cells.

The distinction between feedforward and feedback pathways is somewhat arbitrary from an anatomical point of view because the pyramidal, subpial and stellate cells are potentially involved in both pathways. However, our simulations suggest that the cortex may contain functionally distinct feedforward and feedback pathways. Simulations in which the synapses of pyramidal cells were blocked (effectively an "open-loop" situation) indicate that only the subpial and lateral pyramidal cells are driven by activity in the geniculate afferents. Geniculate inputs to stellate cells are not able to reliably bring the stellate cells to spike threshold. Like stellate and horizontal cells, subpial cells are driven by recurrent excitation from pyramidal cell activity. Subpial cells consequently fire in two phases, an early phase driven by geniculate inputs and a late phase driven by pyramidal cell inputs. They can be viewed as participating in both the feedforward and feedback pathways during different phases of the cortical response.

The Feedforward Pathway Controls Wave Formation and Speed

The origination of waves is controlled by two factors. The first is the balance of the excitatory drive from geniculate afferents to lateral pyramidal cells and the $GABA_A$-receptor mediated inhibition of lateral pyramidal cells by subpial cells. Maximal densities of AMPA receptors postsynaptic to geniculate afferents ranging from 0.5 nS to 3.0 nS produce an initial depolarization of lateral pyramidal cells, but do not produce primary waves. Increasing the maximal density of $GABA_A$ receptors postsynaptic to subpial cells on lateral pyramidal cells above 3.8 nS inhibits the production of a primary wave. The second factor is the strength of the excitatory connections between pyramidal cells. An initial depolarization does not develop into a propagating primary wave if the maximal density of AMPA receptors postsynaptic to pyramidal cell collaterals is below 4.5 nS. This is consistent with the findings of Golomb and Amitai (1997), who conducted both simulation and experimental studies. They used a one dimensional array of neurons modeled as compartments with spike generating mechanisms and found that a critical maximal density of AMPA receptors postsynaptic to interneuronal connections was needed to generate a propagating wave. High concentrations of the non-NMDA receptor antagonist, CNQX, blocked the formation of propagating waves. The NMDA receptors postsynaptic to pyramidal cell collaterals in our large-scale model of turtle visual cortex are not required for the development of a propagating primary wave.

The speed of propagating primary waves in the large-scale model is controlled principally by the same factors that control the origination of the wave. The feedforward geniculate pathway can accelerate the wave via direct excitation of lateral pyramidal cells in the model. Similarly, Senseman (1999) found that wave propagation increased as the luminance of diffuse retinal stimuli was increased in the *in vitro* eye-brain preparation. Mancilla et al. (1998) confirmed that the amplitudes of excitatory postsynaptic potentials presumed to be mediated by geniculate afferents increased as a function of the intensity of diffuse retinal flashes. The AMPA-receptor mediated excitation of pyramidal cells by pyramidal cell collaterals in the large-scale model also increased the speed of primary waves. These results are consistent with the findings of Golomb and Amitai (1997) in rat neocortex who found that wave speed was a monotonically increasing function of AMPA receptor density in their one dimensional array of model neurons. Wave speed in their neocortical slices decreased as the concentration of CNQX in the bath medium was increased. Ermentrout (1998) found that the speed of propagating waves in one-dimensional arrays of neurons depends on the effective rise times of the synapses connecting the neurons, the synaptic footprint or spatial extent of the connections between neurons, the resting membrane potential of the neurons and the spike threshold. In particular, wave speed is a monotonically increasing function of the strength of the synaptic connections. Wave speed is a linear function of synaptic strength in some cases and a function of the square root of synaptic strength in others, depending upon the details of the connection pattern between neurons.

Apparently contradictory results have been obtained when the speed of propagating waves is expressed

as a function of NMDA receptor density. Increasing the NMDA-receptor mediated excitation of pyramidal cells by pyramidal cells in our large-scale model resulted in a slight increase in the speed of primary waves when the maximal density of NMDA receptors postsynaptic to pyramidal cells collaterals was lower than 2.0 nS, but had little effect for higher conductance densities. Consistent with this result, Golomb and Amitai (1997) found that increasing the density of NMDA receptors in their model and bath application of the NMDA receptor antagonist, 2-amino-5-phosphonovaleric acid, had little effect on wave speed in rat neocortical slices. By contrast, Traub et al. (1993) found that blocking NMDA receptors resulted in a 50% decrease in wave speed in rat hippocampal slices. These differences may depend upon the specific ratios of AMPA/NMDA receptor densities used. The resting membrane potentials of neurons is also likely to be significant in that more depolarized membrane potentials would relieve the magnesium block of the NMDA receptors.

Wave speed in our large-scale model is a monotonic decreasing function of the $GABA_A$-receptor density on lateral pyramidal cells postsynaptic to subpial cells. Golomb and Ermentrout (2001, 2002) used a one dimensional network of excitatory and inhibitory model neurons to make a distinction between fast and slow pulses or waves. In fast waves, inhibitory cells fire after or slightly before their neighboring excitatory cells. In slow waves, inhibitory cells lead the firing of excitatory cells. Our results suggest that the waves seen in turtle visual cortex are slow waves with inhibition generated by subpial cells controlling the advancing wave front. Consistent with this, intracellular recordings from presumed pyramidal cells in turtle visual cortex demonstrate that diffuse light flashes presented to the retina of an *in vitro* eye-brain preparation elicit inhibitory postsynaptic potentials (IPSPs) with short latencies (Mancilla and Ulinski, 2001). These IPSPs precede the shortest latency excitatory potentials (EPSPs) recorded in pyramidal cells and likely represent feedforward inhibition that is driven by geniculate afferents. Application of $GABA_A$ receptor antagonists demonstrate that $GABA_A$ receptor-mediated inhibition controls the slope of the rising phases of fast EPSPs. Similarly, Chagnac-Amitai and Connors (1989) found that bath application of the $GABA_A$ receptor antagonist, bicuculline, had a strong effect on the speed of propagating responses in slices of rat somatosensory cortex.

The Feedback Pathway Controls Wave Duration

The duration of primary waves is controlled principally by three factors. First, AMPA-receptor mediated excitation of pyramidal cells collaterals can increase the duration of primary waves. Second, the feedback pathway through stellate cells can decrease the duration of primary waves via the NMDA-receptor mediated excitation of stellate cells and the $GABA_A$-receptor mediated inhibition of pyramidal cells by stellate cells. Third, the feedback pathway through horizontal cells decreases the duration of primary waves via the NMDA-receptor mediated excitation of horizontal cells by pyramidal cells and the $GABA_A$-receptor mediated inhibition of pyramidal cells by horizontal cells. Mancilla (2001 and Ulinski (2001) found that intracortical inhibition controlled the amplitudes of slow responses to retinal light flashes. This inhibition likely depends upon the activation of stellate or horizontal cells by pyramidal cell collaterals. The duration of secondary waves is decreased via the direct excitation of pyramidal cells by AMPA receptors postsynaptic to geniculate afferents on pyramidal cells and increased via AMPA receptor-mediated excitation of pyramidal cells collaterals. The duration of secondary waves is decreased by the NMDA-receptor mediated excitation of either stellate cells or horizontal cells by pyramidal cells and the $GABA_A$-receptor mediated inhibition of pyramidal cells by either stellate or horizontal cells.

Functions of Cortical Waves

Propagating activity is a natural consequence of the excitatory connections between pyramidal cells. The existence of cortical waves does not, therefore, necessarily mean that they subserve any biological function. However, Nenadic et al. (2001) and Du et al. (2005) have shown that the waves in turtle visual cortex can encode information about the positions and speeds of stimuli in visual space. Since the formation and propagation of the waves depends upon the strengths of synapses between the various populations of cortical cells, it is reasonable to hypothesize that synaptic strengths would affect the encoding of information. However, varying the strengths of synapses appeared to have relatively little effect on the encoding of information about the positions of stimuli in visual space. This suggests that the encoding process is relatively robust. However, it is important to note

that our simulations were limited to relatively simple stimuli and that the encoding of more complex stimuli might depend more critically on synaptic strenghts.

Acknowledgments

This study was supported by grants from the Learning in Intelligent Systems and Collaborative Research in Neuroscience programs from the National Science Foundation to B.K. Ghosh and P.S. Ulinski. Ulinski also received funds from the Faculty Research Fund at the University of Chicago.

References

Blanton MG, Shen JM, Kriegstein AR (1987) Evidence for the inhibitory neurotransmitter gamma-aminobutyric acid in a spiny and sparsely spiny nonpyramidal neurons of turtle dorsal cortex. J. Comp. Neurol. 259: 277–297.

Blanton MG, Kriegstein AR (1992) Properties of amino acid neurotransmitter receptors of embryonic cortical neurons when activated by exogenous and endogenous agonists. J. Neurophysiol. 67: 1185–1200.

Bringuier et V, Chavane F, Glaeser L, Fregnac Y (1999) Horizontal propagation of visual activity in the synaptic integration field of area 17 neurons. Science 283: 695–699.

Bower JM, Beeman D (1998) The Book of Genesis, 2nd ed. TELOS, New York.

Chagnac-Amitai Y, Connors BW (1989) Horizontal spread of synchronized activity in neocortex and its control by GABA-mediated inhibition. J. Neurophysiol. 61: 747–758.

Chervin RD, Pierce PA, Connors BW (1988) Periodicity and directionality in the propagation of epileptiform dischargers across neocortex. J. Neurophysiol. 61: 747–758.

Colombe JB, Sylvester J, Block J, Ulinski PS (2004) Subpial and stellate cells: Two populations of interneurons in turtle visual cortex. J. Comp. Neurol. 471: 333–351.

Colombe JB, Ulinski PS (1999) Temporal dispersion windows in cortical neurons. J. Comput. Neurosci. 17: 3894–3906.

Contreras D, Llinás R (2001) Voltage-sensitive dye imaging of neocortical spatiotemporal dynamics to afferent activation frequency. J. Neurosci. 21: 9403–9413.

Derdikman D, Hildesheim R, Ahissar E, Arieli A, Grinvald A (2003) Imaging spatiotemporal dynamics of surround inhibition in the barrels somatosensory cortex. J. Neurosci. 23: 3100–3105.

Du X, Ghosh BK, Ulinski PS (2005) Encoding and decoding target locations with waves in the turtle visual cortex. IEEE Trans. Biomed. Eng. 52: 566–577.

Ermentrout B (1998) The analysis of synaptically generated traveling waves. J. Comput. Neurosci. 5: 191–208.

Ghanzafar AA, Nicoleilis MAL (1999) Spatiotemporal properties of layer V neurons of the rat primary somatosensory cortex. Cerebral Cortex 9: 348–361.

Golomb D, Amitai Y (1997) Propagating neuronal discharges in neocortical slices: Computational and experimental study. J. Neurophysiol. 78: 1199–1211.

Golomb D, Ermentrout GB (2001) Bistability in pulse propagation in networks of excitatory and inhibitory populations. Phys. Rev. Lett. 86: 4179–4182.

Golomb D, Ermentrout GB (2002) Slow excitation supports propagation of slow pulses in networks of excitatory and inhibitory populations. Phys. Rev. E. 65: 061911–061916.

Grinvald A, Lieke EE, Frostig RD, Hidesheim R (1994) Cortical point spread function and long-range lateral interactions revealed by real-time optical imaging of macaque monkey primary visual cortex. J. Neurosci. 14: 2545–2568.

Heller SB, Ulinski PS (1987) Morphology of geniculocortical axons in turtles of the genera *Pseudemys* and *Chrysemys*. Anat. Embryol. 175: 505–515.

Kleinfeld D, Delaney KR (1996) Distributed representation of vibrissa movement in the upper layers of somatosensory cortex revealed with voltage-sensitive dyes. J. Comp. Neurol. 375: 89–108.

Larson-Prior LJ, Ulinski PS, Slater NT (1991) Excitatory amino acid receptor-mediated transmission in geniculocortical and intracortical pathways within visual cortex. J. Neurophysiol. 66: 293–306.

Mancilla JG, Fowler MH, Ulinski PS (1998) Responses of regular spiking and fast spiking cells in turtle visual cortex to light flashes. Vis. Neurosci. 15: 979–993.

Mancilla JG, Ulinski PS (2001) Role of $GABA_A$-mediated inhibition in controlling the responses of regular spiking cells in turtle visual cortex. Vis. Neurosci. 18: 9–24.

Mulligan K, Ulinski PS (1990) Organization of the geniculocortical projection in turtles: Isoazimuth lamellae in the visual cortex. J. comp. Neurol. 296: 531–547.

Nenadic Z, Ghosh BK, Ulinski PS (2002) Modelling and estimation problems in the turtle visual cortex. IEEE Trans. Biomed. Eng. 49: 753–762.

Nenadic Z, Ghosh BK, Ulinski PS (2003) Propagating waves in visual cortex: A large-scale model of turtle visual cortex. J. Comput. Neurosci. 14: 161–184.

Petersen CCH, Sakmann B (2001) Functionally independent columns of rat somatosensory barrel cortex revealed with voltage-sensitive dye imaging. J. Neurosci. 21: 8435–8446.

Petersen CCH, Grinvald A, Sakmann B (2003) Spatiotemporal dynamics of sensory responses in layer 2/3 of rat barrel cortex measured *in vivo* by voltage-sensitive dye imaging combined with whole-cell voltage recordings and neuron reconstructions. J. Neurosci. 23: 1298–1309.

Prechtl JC, Bullock TH, Kleinfeld D (2000) Direct evidence for local oscillatory current sources and intracortical phase gradients in turtle visual cortex. Proc. Natl. Acad. Sci. 97: 877–882.

Prechtl JC, Cohen LB, Mitra PP, Pesaran B, Kleinfeld D (1997) Visual stimuli induce waves of electrical activity in turtle visual cortex. Proc. Natl. Acad. Sci. 94: 7621–7626.

Robbins KA, Senseman DM (2004) Extracting wave structure from biological data with application to responses in turtle visual cortex. J. Comput. Neurosci. 16: 267–298.

Seidemann E, Arieli A, Grinvald A, Slovin H (2002) Dynamics of depolarization and hyperpolarization in the frontal cortex and saccade goal. Science 305: 862–865.

Senseman DM (1999) Spatiotemporal structure of depolarization spread in cortical pyramidal cell populations evoked by diffuse retinal light flashes. Vis. Neurosci. 16: 65–79.

Senseman DM, Robbins KA (2002) High-speed VSD imaging of visually evoked cortical waves: decomposition into intra- and intercortical wave motions. J. Neurophysiol. 87: 1499–1514.

Traub RD, Wong RKS, Miles R, Michelson H (1991) A model of a CA3 hippocampal pyramidal neuron incorporating voltage-clamp data on intrinsic conductances. J. Neurophysiol. 66: 635–650.

Traub RD, Jefferys JGR, Miles R, Michelson H (1993) Analysis of the propagation of disinhibition-induced afer-discharges along the guine-pig hippocampual slice *in vitro*. J. Physiol. (Lond.) 472: 267–287.

Ulinski PS (1986) Organization of the corticogeniculate projections in the turtle, Pseudemys scripta. J. Comp. Neurol. 254: 529–542.

Ulinski PS (1999) Neural mechanisms underlying the analysis of moving visual stimuli. In: Ulinski PS, Jones EG, Peters A, eds. Cerebral Cortex. Vol. 13. Models of Cortical Circuitry. Plenum Press, New York, pp. 283–399.

Wang W (2006) Dynamics of the turtle visual cortex and design of sensor networks. D.Sc. thesis. Washington University, Saint Louis, MO.